Prediction and control of combustion instabilities in real engines

Thierry Poinsot

Prediction and control of combustion instabilities in real engines

T. Poinsot [a,b,c,*]

[a] *IMF Toulouse, INP de Toulouse and CNRS, Toulouse 31400, France*
[b] *CERFACS, Toulouse 31057, France*
[c] *Center for Turbulence Research, Stanford, CA 94305, USA*

Abstract

This paper presents recent progress in the field of thermoacoustic combustion instabilities in propulsion engines such as rockets or gas turbines. Combustion instabilities have been studied for more than a century in simple laminar configurations as well as in laboratory-scale turbulent flames. These instabilities are also encountered in real engines but new mechanisms appear in these systems because of obvious differences with academic burners: larger Reynolds numbers, higher pressures and power densities, multiple inlet systems, complex fuels. Other differences are more subtle: real engines often feature specific unstable modes such as azimuthal instabilities in gas turbines or transverse modes in rocket chambers. Hydrodynamic instability modes can also differ as well as the combustion regimes, which can require very different simulation models. The integration of chambers in real engines implies that compressor and turbine impedances control instabilities directly so that the determination of the impedances of turbomachinery elements becomes a key issue. Gathering experimental data on combustion instabilities is difficult in real engines and large Eddy simulation (LES) has become a major tool in this field. Recent examples, however, show that LES is not sufficient and that theory, even in these complex systems, plays a major role to understand both experimental and LES results and to identify mitigation techniques.

Keywords: Instabilities; LES; Thermoacoustics; Gas turbines

1. Introduction

Most combustion systems are designed to operate in stable regimes. However, all experimentalists working on steady combustion chambers (furnaces, gas turbines, power plants) know that 'sometimes', a chamber starts exhibiting unexpected oscillations. These combustion instabilities (often called thermoacoustic) lead to additional noise and vibration, which can be ignored or tolerated if the level of oscillations remains small (less than a few mbars). In other cases, however, pressure fluctuations can reach values of the order of a large fraction of

* Correspondence to: IMF Toulouse, INP de Toulouse and CNRS, 31400 Toulouse, France
E-mail address: thierry.poinsot@cerfacs.fr

the mean pressure and lead to more serious consequences: the chamber can quench, the flame can flashback and burn part of the injection system. The pressure oscillations can also become large enough to damage the combustor structure or lead to the explosion of the engine.

Combustion instabilities (CIs), also called flame dynamics, are an important field of combustion research. It combines all usual sciences involved in reacting flows (kinetics, transport, fluid mechanics, thermodynamics) but also requires the introduction of acoustics, hydrodynamic stability, dynamical systems and control theory. Even though CIs can appear in almost any combustion system, industry is not especially keen on studying them or in recognizing that they can be a problem in their company's engines. The main reason for this is that CIs are the cause of major problems, which are difficult to master because they occur during the last stages of development and are still difficult to predict today: having an unstable engine is still similar to catching some kind of disease for companies. Since the adventure of the F1 engine during the Apollo program in the 60s, which cost billions of dollars before a solution was found to mitigate CIs [1], companies know that CIs are a major industrial risk, for which communication may not be the best solution. CIs have been the hidden and feared problem of many combustion programs, starting with solid and liquid fuel rocket engines in the 50s and continuing more recently in gas turbines, industrial furnaces or even domestic heaters.

Laboratories, on the other hand, have no difficulty studying instabilities in canonical cases such as laminar premixed flames and the literature contains a very large amount of research work dedicated to CIs in simple flames [2–9]. When it comes to real engines,[1] the situation is different. Here, CI mechanisms involve not only those found in academic experiments, but also introduce new physics that is usually not studied in laboratories:

- Real flames are turbulent and many of them are swirled and confined in complex shape chambers. CIs in turbulent swirled flames are now commonly studied in laboratories [10–18] but usually in simplified chambers that do not contain the complexities found in real engines.
- Power density is known to be an important parameter for instabilities: when combustion chambers become smaller or when their power increases, CIs are more prone to appear. This usually occurs for high-pressure systems, which are more difficult to study in laboratories. The best example is transverse modes in rocket engines [19,20], which appear on real systems but are difficult to trigger in laboratory set-ups, which are scaled down in terms of pressure and power density [21–23].
- Most laboratories study instabilities in gaseous flames. Even if research on CIs actually started in the 50s for liquid-fueled systems [24–26], studying instabilities in liquid fueled combustors is much more complicated [27,28].
- The geometry of the chamber is a first-order parameter for CIs: in gas turbines, combustion chambers have annular shapes where azimuthal instability modes can develop, something that had never been studied in laboratories until very recent times [29–31] for obvious cost reasons. Therefore the physics of azimuthal modes was known mainly on the basis of limited experimental observations performed on real full turbines [32–34].
- Laboratory burners use single injection systems, which create isolated flames. Gas turbines chambers can have twenty injectors and flames. Rocket chambers feature hundreds of injectors: therefore flame/flame interactions are dominant in real engines and absent in most laboratory burners.
- Most instability modes studied in laboratories involve longitudinal acoustic modes, which propagate along the flow direction. In real engines, modes can also be transverse, radial or azimuthal. More importantly, modes can be much more numerous than in a laboratory experiment because real configurations are geometrically complex. An industrial gas turbine can exhibit 30 acoustic eigenmodes between 0 and 250 Hz, many of them having the capacity to become self-excited [34]. This never happens in laboratory systems, which are much simpler. Being able to recognize which mode appears in such a system becomes significantly more complicated than in a laboratory scale experiment, where only a few modes can be found and are easily identified by their frequencies.
- Many unstable modes studied in laboratories correspond to situations where entropy waves play a limited role. In chambers terminated by a nozzle or by a stator/rotor stage, entropy waves can be reflected back as acoustic waves into the chamber, creating a new class of CI, called entropy - acoustic modes. Fluctuations of equivalence ratio are also encountered in many real engines, where they can induce specific CI modes.
- Finally, simple, well-defined inlet and outlet conditions (imposed pressure or imposed velocity) can be imposed to control acoustic reflections in laboratory combustors (Section 4.3). This is different in real engines.

[1] The term 'real engine' will be used here to designate engines used in real industrial systems, as opposed to chambers studied in laboratory environments.

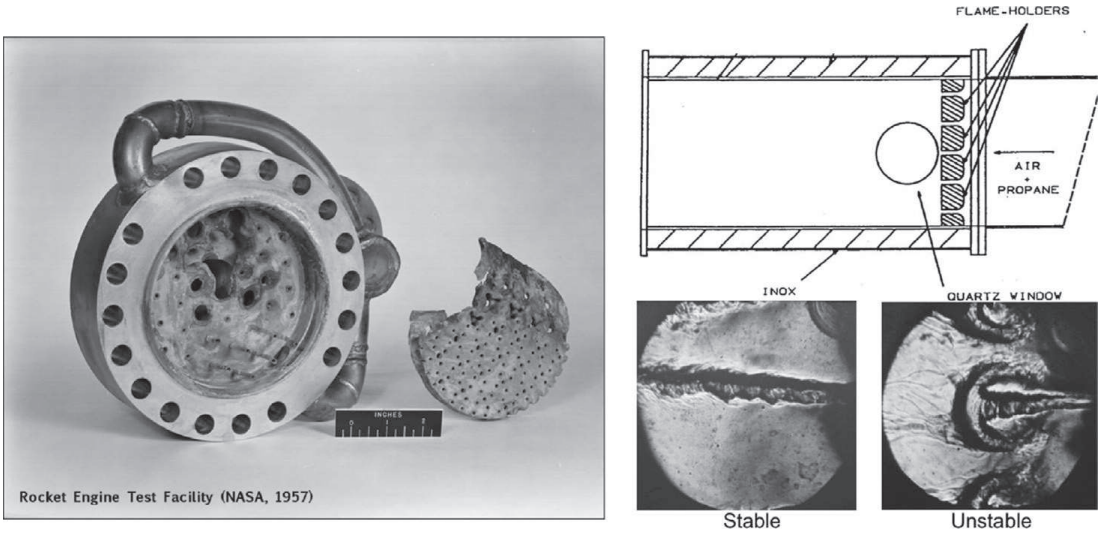

Fig. 1. Rocket engine destroyed by instability during the early years of the US rocket program (left) and a laboratory burner exhibiting both stable and unstable regimes (right) [38].

In gas turbines, for example, the chamber is fed by a compressor and blows into a turbine. Determining the impedances of these elements is a daunting task in itself.

This review discusses combustion instabilities appearing in engines. Its objective is to describe modern simulation methods combined with new experiments and theoretical developments for such instabilities. Readers are referred to other reviews for complete descriptions of instability mechanisms [20,35–37]. Of course, the presentation builds on fundamental results obtained for CIs in laboratories over the last hundred years but its main goal is to discuss what must be added to these elements when real engines are considered.

Thermoacoustic CIs are due to coupling mechanisms between unsteady combustion and acoustic waves propagating in the chamber and reflecting on its walls, inlets and outlets.[2] The left image of Fig. 1 shows a NASA rocket engine partially destroyed after the engine encountered CI while the right picture displays high-speed views of the flow in a laboratory premixed burner for a stable and an unstable regime [38]: the instability changes the flow drastically, creating mushroom-shaped vortices at a frequency of 530 Hz and a very short and intense turbulent flame that can destroy the chamber in a few minutes.[3]

From a fundamental point of view, CIs constitute one of the most challenging problems in fluid mechanics: they combine turbulence, acoustics, chemistry and unsteady two-phase flow in complex geometries. The scales to capture vary from the laminar flame thickness (less than 0.1 mm) to the acoustic wavelengths (a few meters) and the speeds from flame speeds (less than 1 m/s) to the sound speed (more than 600 m/s in the burnt gases). Computing CIs is more difficult than computing steady combustion and requires more sophisticated tools because they must capture unsteady phenomena and unstable mechanisms. The intensity of the acoustic field generated by a flame in the absence of CI is small: the acoustic power created by a combustor is typically less than 10^{-8} times the combustor power. Predicting precisely the acoustic field created by a flame is much more difficult than simulating the flame itself [39,40]. Even if such a small conversion factor from mechanical energy to sound leads to a relatively small level of energy contained in the acoustic field, these acoustic fluctuations can have a strong effect on the flames themselves, closing a resonant feedback loop which is difficult to predict: capturing flame / acoustic coupling to predict self-sustained instabilities is one of the overarching simulation problems in the combustion community.

The basic mechanisms leading to combustion instabilities were identified 150 years ago by Lord Rayleigh [41] but they have become real research topics as well as practical dangers for many industrial programs when the power density of combustion chambers has increased sufficiently, first in rocket [24] and later in jet engines [19,42,43]. Studies of combustion instabilities and noise are numerous [24,26,44–53] and started long ago [41]. A flame is not needed to produce such coupling: as shown by Rijke [54,55], a heated gauze placed in a tube is enough to produce a “singing” tube caused by the coupling between the acoustic modes of the duct and the unsteady heat released by the gauze [56,57].

[2] Most unconfined flames do not exhibit strong combustion instabilities.

[3] In a real combustor, this can be much faster: a fighter-aircraft engine submitted to screech, a strong CI mode, or a rocket engine where a transverse mode grows can explode in a few seconds.

However, when the heat release is due to a flame, more energy can be transmitted into the acoustic field and the effects of combustion instabilities are much more dangerous.

CIs are also known under other names such as thermoacoustics in flames or combustion dynamics: the Hottel lecture of S. Candel in 2002 [35] provides a precise history of CI research and of methods used to control them. The books of Lieuwen and Yang [36] and Culick [19] describe CI physics in multiple real combustion systems. The objective of the present lecture is not to repeat these excellent reviews but to complement them by discussing important progress achieved in the last 10 years in the field of CI modeling and simulation. A major revolution in this domain has been the introduction of LES methods for CI computations. LES has become one essential tool to analyze CIs but, as shown in the next sections, it is not sufficient to fully analyze CI: like experiments, LES can tell whether a given combustor will be unstable but it does not tell why this is so and how we can control this instability. To understand why instabilities appear and how to control them, other approaches are needed such as theory and simplified simulation tools (linearized Euler equations, for example), which will be discussed in the next sections.

The present paper focuses on gas turbines: they provide excellent examples of CIs that require more studies than laboratory systems because they lead to completely new physics. First, a simple pedagogical model of dump combustor is described to recall classical coupling mechanisms between flames and acoustics and introduce stability criteria (Section 2.1). Simulation methods for CIs are presented in Section 2.2, before applying them to the specific case of gas turbine engines in Section 3, which discusses recent LES and experimental results on annular chambers. The configurations that will be presented, are typical of gas turbine engines (Section 3.1) and they exhibit azimuthal modes that cannot be observed in usual laboratory set-ups. Recently, theory has been introduced with significant success to analyze these modes (Section 3.2). CI control methods in annular chambers have also become a topic in itself, that is discussed in Section 3.3. After this section, the presentation opens to new topics that are relevant for annular chambers but to other engines as well (Section 4): the coupling between wall heat transfer and CIs (Section 4.1), the recent discovery of intrinsic acoustic modes (Section 4.2), the need to consider impedances to analyze CIs (Section 4.3, which is critical for gas turbines), recent results on hydrodynamic stability of swirled flows (Section 4.4) and the existence of flame bifurcations in swirled combustors that can be triggered by CIs (Section 4.5). Finally, the need to introduce UQ (Uncertainty Quantification) for CI studies is the topic of Section 4.6.

2. Modeling and computing combustion instabilities

2.1. A model problem illustrating key features of combustion instabilities

Most CIs are due to a resonance between unsteady combustion processes and acoustic waves propagating in the combustion chamber. The mechanisms leading to an amplification of combustion/acoustic processes are best explained by beginning with the simple model problem described in Fig. 2. Consider a constant cross-section duct where a flame is stabilized at the dump plane separating the injection tube (length l_1, section S_1) and the combustion chamber (length l_2, section S_2).

For low-frequency longitudinal modes, planar acoustic waves propagate both in the injection tube and the chamber so that the fluctuating acoustic pressure (p'_i) and velocity (u'_i) signals in these two ducts (numbered $i = 1$ to 2, $x = 0$ corresponds to the flame position) are:

$$u'_i(x,t) = \frac{1}{\rho_i c_i} Re\left(\left[A_i^+ e^{jk_i x} - A_i^- e^{-jk_i x}\right] e^{-j\omega t}\right) \qquad (1)$$

$$p'_i(x,t) = Re\left(\left[A_i^+ e^{jk_i x} + A_i^- e^{-jk_i x}\right] e^{-j\omega t}\right). \qquad (2)$$

where $k_i = \omega / c_i$ is the wave number in duct i, ω the pulsation and c_i the sound speed in duct i. To determine the acoustic wave amplitudes A_1^-, A_1^+, A_2^- and A_2^+, boundary conditions are imposed at the inlet (usually $u'_1 = 0$ because velocity is imposed) and at the outlet (usually $p' = 0$ for chambers open

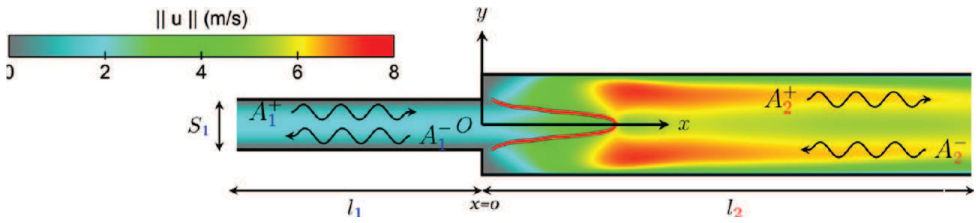

Fig. 2. A simple pedagogical model for combustion instabilities: a laminar flame stabilized at the dump plane separating the injection duct and the combustion chamber. The color field is the velocity modulus [58].

to the atmosphere where pressure is constant). At the dump plane where the flame is stabilized, jump conditions from one side of the flame to the other allow to relate pressure and velocity perturbations on both sides of the flame front, assuming that the flame is compact compared to the acoustic wavelength. Through such a compact flame, pressure perturbations are conserved while the unsteady volume flow rate increases because of the total unsteady heat release in the flame $\dot{\Omega}'$ [49,59,60]:

$$p_2'(x=0,t) = p_1'(x=0,t) \quad \text{and}$$
$$S_2 u_2'(x=0,t) = S_1 u_1'(x=0,t) + \frac{\gamma-1}{\rho_1 c_1^2}\dot{\Omega}' \tag{3}$$

where ρ_j is the mean density in section j and γ the ratio of specific heats. A convenient scaling for $\dot{\Omega}'$ is to express it as a function of the chamber inlet velocity fluctuations u_1', as proposed by Crocco [24] who introduced an interaction indeed n (measuring the strength of the flame response) and a time delay τ (measuring the time required by the flame to react to forcing):

$$\frac{\gamma-1}{\rho_1 c_1^2 S_1}\dot{\Omega}' = n u_1'(x=0, t-\tau) \tag{4}$$

so that, assuming harmonic variations for all perturbations $f' = \hat{f} e^{-j\omega t}$, jump conditions become:

$$\hat{p}_2(x=0,t) = \hat{p}_1(x=0,t) \quad \text{and}$$
$$S_2 \hat{u}_2(x=0,t) = S_1 \hat{u}_1(x=0,t)(1+ne^{j\omega\tau}) \tag{5}$$

Eq. (4) is the heart of most CI models: it allows linking heat release fluctuations (due to convective and chemical effects) to a single acoustic velocity at the chamber inlet ($x=0$). Once it is accepted, there is no need to solve for any other mechanisms except than acoustics. The whole problem of CI becomes an acoustic problem only, and Eq. (3) together with boundary conditions at the inlet (constant velocity at $x=-l_1$, which imposes $A_1^+ e^{jk_i l_1} - A_1^- e^{-jk_i l_1} = 0$) and at the outlet (constant pressure at $x=l_2$, which imposes $A_2^+ e^{jk_i l_2} + A_2^- e^{-jk_i l_2} = 0$) leads to an homogeneous equation for the wave amplitudes A_1^-, A_1^+, A_2^- and A_2^+, which has a non-zero solution only if:

$$\cos\left(\omega\frac{l_2}{c_2}\right)\cos\left(\omega\frac{l_1}{c_1}\right) - \Gamma\sin\left(\omega\frac{l_2}{c_2}\right)\sin\left(\omega\frac{l_1}{c_1}\right)$$
$$\times(1+ne^{j\omega\tau}) = 0 \quad \text{with} \quad \Gamma = \frac{\rho_2 c_2}{\rho_1 c_1}\frac{S_1}{S_2} \tag{6}$$

Eq. (6) is a dispersion relation for ω: the real part of ω is the pulsation of the mode that will occur in a CI oscillation; its imaginary part provides the growth rate. If it is positive, this model predicts that the mode will be linearly amplified, leading to CI. Of course, this linear approach cannot predict the amplitude of the limit cycle that might be reached after the mode starts growing, but the previous demonstration shows that the essence of CI can be described in only a few lines.

The general solution of Eq. (6) is difficult to express but an analytical expression is easily obtained in a simplified case where the tubes have the same sections and lengths ($S_2 = S_1$ and $l_2 = l_1 = a$) and the flame induces a negligible heat release so that $\rho_2 = \rho_1$ and $c_2 = c_1 = c$. In this case, $\Gamma = 1$ and the dispersion relation becomes $\cos^2(\omega a/c) - sin^2(\omega a/c)(1+ne^{j\omega\tau}) = 0$. In the absence of flame ($n=0$) the solution of the dispersion equation simply corresponds to the acoustic eigenmodes of a duct of length $2a$: the first mode is such that $k_o l = \pi/4$. It has a zero growth rate ($\Im(k_o) = 0$) and a wave length $\lambda_0 = 2\pi/k_o = 8a$ (four times the total length of the duct $2a$) explaining why this mode is called the quarter-wave mode. Its period is $T_o = 2\pi/\omega_o = 8a/c$.

If the flame is active and n is non zero but still small, the solution for k can be written as a Taylor expansion around k_o so that $k = k_o + k'$ with:

$$Re(k) = \pi/(4a) - \frac{n}{4a}\cos(2\pi\tau/T_o) \quad \text{and}$$
$$\Im(k) = \Im(k') = -\frac{n}{4a}sin(2\pi\tau/T_o) \tag{7}$$

Since n is small in this approach, the pulsation of the mode ($Re(k)/c$) is only weakly affected by the flame effect: the unstable mode frequency remains close to the quarter-wave frequency without active flame. The active flame ($n \neq 0$), however, controls the growth rate of the mode: the combustor will be unstable if $\Im(k) > 0$, which implies here $\sin(2\pi\tau/T_o) < 0$ or $(p+1/2)T_o < \tau < (p+1)T_o$ where p is an integer. This instability criterion indicates that certain values of the flame delay τ will lead the flame to instability. For the first mode ($p=0$), the delay τ must be larger than the half-period T_o of the first acoustic mode and less than T_o:

$$T_o > \tau > \frac{1}{2}T_o \tag{8}$$

Even if the assumptions used to derive this stability criterion are crude, this analysis contains all the ingredients of many low-order models used for thermoacoustics:

- It requires all convective and chemistry effects to be modeled as a function of a purely acoustic quantity (which must be either pressure or acoustic velocity). Here the Crocco model was used where the unsteady reaction rate $\dot{\Omega}'$ is expressed as a function of the acoustic velocity at the chamber inlet $u_1'(x=0,t)$. More sophisticated models may be found in the literature [6,61,62]. Most of them assume that $\dot{\Omega}'$ depends on previous values of the reference velocity $u_1'(x=0)$. This dependence is usually expressed through a flame transfer function (FTF) F, depending

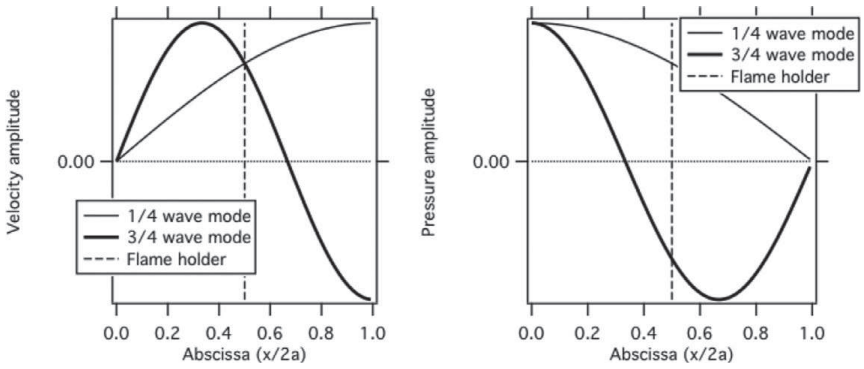

Fig. 3. The structure of the 1/4 and 3/4 wave modes in the model of Fig. 2.

on the pulsation ω:

$$\dot{\Omega}'/\bar{\dot{\Omega}} = F(u_1'(x=0, t*; t* < t)/\bar{u}(x=0)) \tag{9}$$

The FTF can also depend on the amplitude of the oscillation A in which case it is called an FDF (Flame Describing Function) [63–65]. In many combustors, the fresh gases velocity may not be the only quantity affecting unsteady combustion. The fluctuations of equivalence ratio ϕ at the chamber inlet have been identified as another important control parameter [66–68] so that present expressions for FDF are often written as:

$$\dot{\Omega}'/\bar{\dot{\Omega}} = F(u_1'(x=0, t)/\bar{u}(x=0), \phi'/\bar{\phi}, A) \tag{10}$$

- The previous derivation was performed for the first acoustic mode (1/4 wave) but other higher-order modes can be amplified too. In the model of Fig. 2, those are the 3/4, 5/4... modes. In most chambers, only the lowest order acoustic modes are expected because the acoustic dissipation increases rapidly with mode order and frequency.
- It leads to a stability criterion that depends on τ (and weakly on n) in most cases. When k is determined, the mode structures (i.e. the dependence on p' and u' on spatial coordinates) can be obtained too. As an example, Fig. 3 displays the structure of the first two modes (1/4 and 3/4 wave).

2.2. Classification of simulation methods for combustion instabilities

Two main classes of techniques are used to simulate combustion instabilities (Fig. 4): the first category; and the only one until the 2000s, is thermoacoustic codes (called TA here) in which flames are not simulated but replaced by their equivalent FTF or FDF [69–72]. The mean flow is frozen and solutions are sought for the linearized perturbations. The toy model of Fig. 2 is an example of such an approach in a one-dimensional case. More sophisticated methods can be developed in three dimensions, in time or Fourier space but they all share the same basic idea: avoiding the complexity of flow and chemistry by lumping all their effects into some form of FDF.

FTFs and FDFs required for TA modes can be obtained analytically in simple cases [9,40,73], or experimentally [64,74]. To complement these approaches, a second class of methods was introduced around 2000 to compute explicitly the flame dynamics, using full LES of the forced reacting flow [14,75,76]. This is more expensive and it raises various difficulties to handle acoustic boundary conditions, chemistry, turbulence... LES can be used for CI studies in two modes: brute force LES consists in setting a computational domain as large as possible (e.g. accounting for all geometrical parts of the engine), matching all boundary conditions (including impedances at exits and inlets) and letting the LES solver compute the self-excited instabilities of the combustor. The second method (called forced open-loop LES) uses LES only to compute the FTFs of a given flame and provide this information as input data for TA codes. Both approaches will be used in the present review.

3. Azimuthal modes in gas turbines

While laboratory studies have been mostly limited to cylindrical or parallepipedic combustion chambers fed by a single burner, real systems such as gas turbines use annular geometries for combustion and feed them with multiple burners ($N = 10$ to 24). From a thermoacoustic point of view, this introduces two new types of physics:

- Since the combustion chamber is an annulus, azimuthal acoustic modes due to acoustic waves traveling along the two azimuthal directions (clockwise (CW) and anticlockwise (ACW)) can become unstable.
- Instead of considering the response of a single burner to longitudinal acoustic modes, annular chambers require to understand how

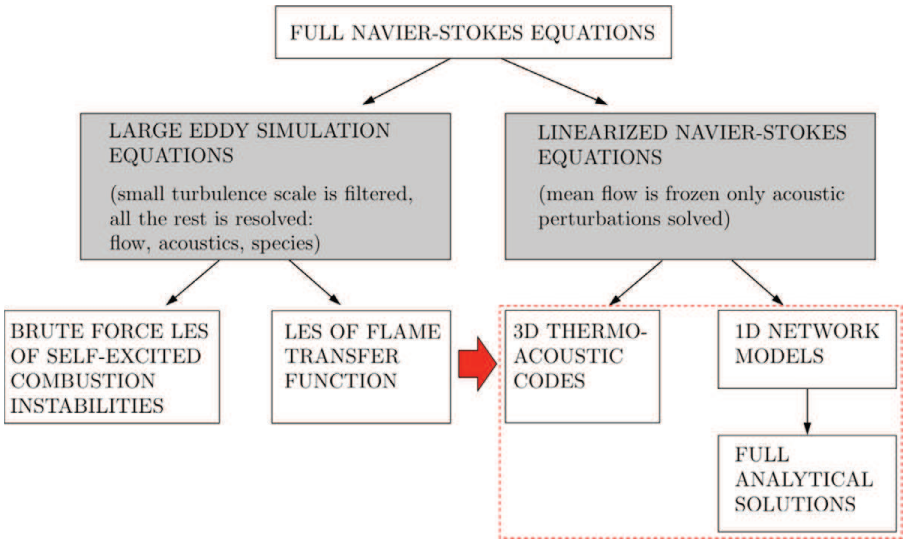

Fig. 4. Simulation methods for combustion instabilities.

N burners can couple with the acoustic field.

Since the perimeter of most annular chambers is of the same order as their length, azimuthal and longitudinal modes develop in similar frequency ranges [34,36,59,71]: being able to distinguish these modes by looking at their frequencies only is impossible. A second specificity of azimuthal modes is their nature: the acoustic waves developing in the annular chamber can be standing (with certain burners being submitted to zero pressure fluctuations at nodes while others located near antinodes experience large pressure oscillations) or turning (in which case, all burners in the chamber see the same pressure fluctuation levels). This has been recognized and discussed in many past studies since the works of companies like Siemens [34] or Alstom [77], who showed that both spinning and standing azimuthal modes were observed in an annular gas turbine. In 2002, Krebs et al. [34] showed experimentally that the modes identified in a real gas turbine were sometimes turning, sometimes standing and could transition from one state to another for the same operating point.

Even if the question of the mode structure (standing vs turning) is an exciting one from the point of view of stability and chaos theories, the practical question is more to know how to eliminate these modes rather than to understand them. In the 1990s, active control was shown to be an effective way to control unstable modes in combustion chambers [78–80], including annular chambers [81]. However, the cost and the certification difficulties have shown that it was more interesting to build combustors that would be stable by design rather than trying to control them with active systems. The next sections describe some of the recent theories in this direction. These efforts include LES but also new experiments and theory.

3.1. Azimuthal instability modes in annular chambers

Five years ago, the development of powerful LES techniques for reacting flows [14,76,82,83] applied to full annular combustors [84,85] confirmed that azimuthal modes could change nature randomly, evolving from spinning to standing structure at random instants. Fig. 5 displays an example of annular geometry (only one sector with one burner is shown for clarity) and instantaneous pressure and velocity fields for an unstable helicopter engine configuration. The pressure field is turning, modifying combustion in each sector and feeding the instability mechanism.

Interestingly, LES showed right away that the mode nature was changing with time: in the same LES, without any parameter change, the mode would alternate between standing and turning characteristics. After LES revealed that azimuthal modes could be captured numerically, new experiments were also developed [30,86], confirming LES results and showing that azimuthal modes could be reproduced in a laboratory environment and that they were indeed intermittent and switching from one type to another. Fig. 6 shows the experimental configuration of Cambridge [30,87] (left image) and an example of structure analysis (right image). This analysis uses multiple microphones located along the azimuthal direction to measure the acoustic waves amplitudes turning clock wise (called $A-$) and anticlockwise ($A+$). When one of these two waves dominate the other, the mode is turning. When the two waves have similar amplitudes, the mode is standing. The scatter plot of Fig. 6 reveals a wide distribution of the proba-

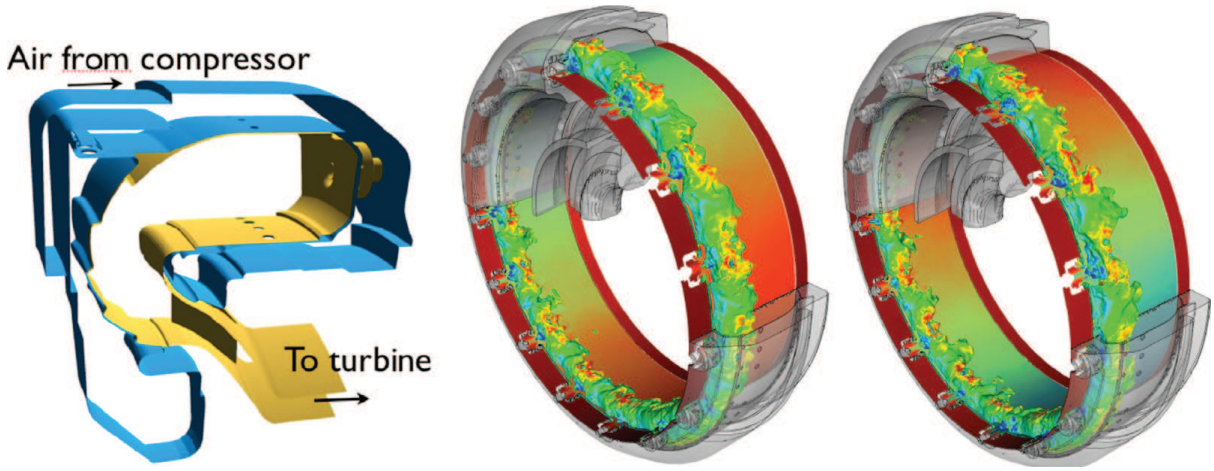

Fig. 5. LES of the first azimuthal unstable mode in an helicopter engine [84,85] . Left: geometry of a single sector. Right: two snapshots of pressure on a cylinder passing through the burner axis and isosurfaces of temperature colored by axial velocity.

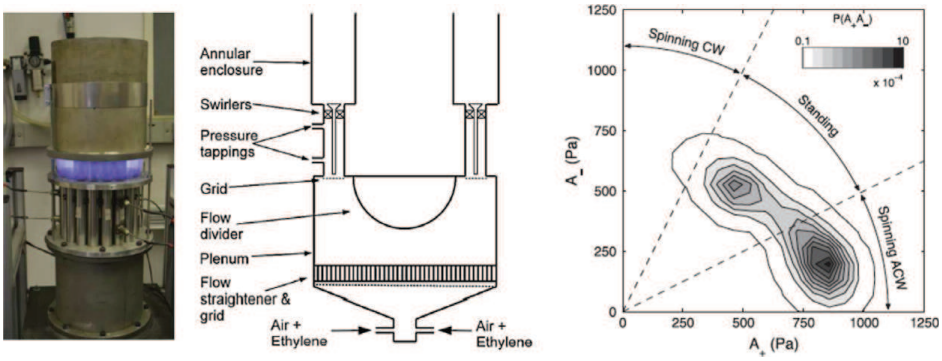

Fig. 6. Cambridge annular chamber [87,92]. Left and center: configuration. Right: joint pdf of mode state in terms of clockwise and anticlockwise wave amplitudes.

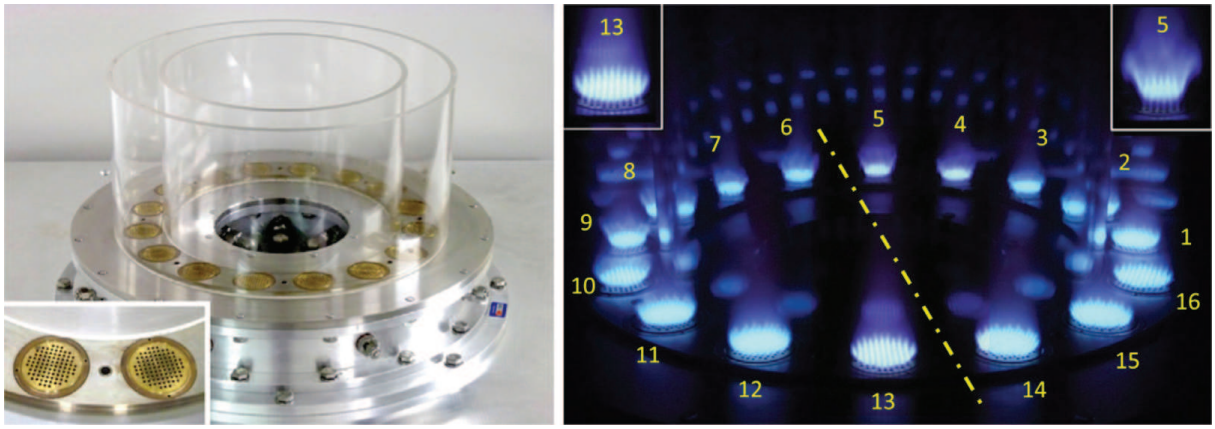

Fig. 7. EM2C annular chamber [31,93]. Left: configuration. Right: slanted mode visualization. In the foreground (burner 13), flames are stuck on the grids. In the back (burner 5), the flames are blown off at the periphery of the grids.

bility density function of the chamber state defined by $(A-, A+)$ doublets. Various theories have been proposed to understand this type of results [77,88–91] but the issue is still open.

Experiments rapidly raised additional questions: for example, triggering azimuthal modes proved to be difficult because longitudinal modes would often grow faster than azimuthal modes. Furthermore, unexpected factors such as the respective lengths of the chamber inner and outer tubes seemed to control the existence of azimuthal modes.

Spinning and standing modes were not the only modes that were discovered experimentally. A 'slanted' mode was reported by the EM2C group [31] in an annular chamber fed by matrix grids. This mode at 450 Hz is a combination of two modes with coinciding frequencies, the first one being a standing azimuthal mode and the second one, an axial mode. Half of the flames (foreground of Fig. 7) are oscillating in a limited way and remain stuck to the matrix injection systems while the other side (background of Fig. 7) are more unstable and lift from the matrix: burners like number 5 or 13, for example, exhibit very different mean flame shapes. No analytical method or simulation has been able to predict this mode for the moment.

Studying azimuthal modes in annular chambers requires to investigate a new generic problem: the response of flames to transverse velocity fluctuations. Indeed, these modes create oscillating velocities that are normal to the flow (unlike usual longitudinal modes). Such a transverse forcing can actually be created in laboratory experiments that are similar to the ones used for FTF of flames submitted to longitudinal waves, except that, for transverse forcing, waves are produced by lateral loudspeakers to induce velocity fluctuations normally to the flow axis [20,94–97]. These set-ups demonstrate that the flame response depends on the nature of the flame position in terms of acoustic field. If the flame is located near a pressure antinode, it will sense mainly axial flow rate oscillations and its response will be similar to the one obtained though axial forcing. If the flame sits at a velocity antinode, it will be submitted to strong transverse movements, which have a limited effect on the unsteady heat release when flames do not interact (since the flame is only oscillating around it mean position). Neighboring flames interaction (something that cannot be studied with the experiments of Lespinasse et al. [94,98] or of O'Connor et al. [95]) might lead to stronger pulsations of heat release and can be studied only in full 360 degree combustors [30].

3.2. *Analytical methods for azimuthal instability modes*

A major limitation of both experimental and LES studies in this field is cost. A second one is that even if they allow us to capture azimuthal modes, they do not provide information on mechanisms and on possible control strategies. Therefore, simpler tools (TA class of Fig. 4) are needed to explore azimuthal CIs basic nature and this has to be done in idealized configurations. Such tools can be built using network approaches and fully analytical methods [20,53,99,100]. Recently, analytical studies have progressed in two directions: 1) Linear theories are based on network models [99–102]. The acoustic-flame behavior is assumed linear and modeled by a Flame Transfer Function (FTF) while major features of the configuration are retained such as complex burners, including an annular plenum and a chamber, taking into account a mean azimuthal flow etc. These studies can determine the stability of the configuration but also predict linear effects on mode structure. 2) Nonlinear approaches usually based on Galerkin methods [77,91], where the configuration is reduced to a simple annulus with zero or an infinite number of burners and no plenum, but the acoustic-flame behavior can be more complicated and integrate non-linear effects using a Flame Describing Function (FDF), allowing the investigation of limit cycles.

As an example of the power of analytical tools, the ATACAMAC approach [99,101] is described here. ATACAMAC describes acoustic waves propagation in an annular chamber as a network of one-dimensional ducts where flames create jump conditions for velocities. It is a direct extension of the model of Section 2.1: here, N burners (instead of a single one for Section 2.1) feed a 1D annular chamber (Fig. 8). In the chamber, between two burners, simple acoustic propagation takes place with two co- and counter- rotating waves. At the junctions between chamber and burner, jump conditions can be written. The length and section of the ith burner are noted L_i and S_i while the perimeter and the cross-section of the annular chamber are $2L_c = 2\pi R_c$ and S_c respectively. Points in the burners are located using the axial coordinate z where $z = 0$ designates the upstream end and $z = L_i$ the burner/chamber junction. The ith compact flame location is given by the normalized abscissa $\alpha = z_{f,i}/L_i$. An impedance Z is imposed at the upstream end of each burner ($z = 0$). Subscript c corresponds to the chambers and subscript u to the unburnt gases upstream of the flame in the burners. Unsteady combustion is modeled using an FTF for each flame: in each burner, the unsteady heat release depends linearly on the acoustic velocity upstream of the flame in the corresponding burner (Eq. (4)).

For small values of n, a fully analytical solution can be obtained for the eigenmodes by a Taylor expansion around the mode that exists in the absence of active flame ($n_i = 0$). Theory shows first that the single most important parameter controlling stability is the set of the N coupling parameters Γ_i given by:

$$\Gamma_i = \frac{1}{2}\frac{S_i\rho^0 c^0}{S_c\rho_u^0 c_u^0} tan(k_u L_i)\left(1 + n_i e^{j\omega\tau_i}\right) \tag{11}$$

where $k_u = \frac{\omega}{c_u}$ and (n_i, τ_i) are the interaction index and the time-delay of the FTF for the ith flame. Eq. (11) corresponds to a case where $Z = \infty$ (the inlet velocity of the burners is fixed). If all burners are identical, all Γ_i's are equal.

The expression of the frequencies of the two first azimuthal modes (clockwise and anticlock-

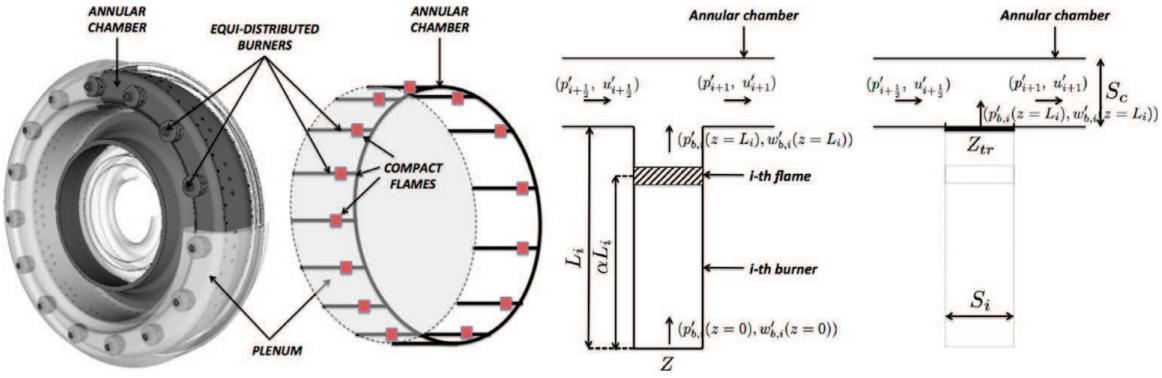

Fig. 8. Analytical model [99,101] to study unstable modes in annular chambers with a steady and uniform azimuthal flow (constant Mach number M_θ). Left: modeling a full turbine by a network of 1D elements. Right: replacing burners by a translated impedance on the chamber walls.

wise) is:

$$f_{CW} = \frac{c_c}{2L_c} - \frac{c_c}{4\pi L_c}(\Sigma + \mathcal{S}_0) \quad \text{and}$$
$$f_{ACW} = \frac{c_c}{2L_c} - \frac{c_c}{4\pi L_c}(\Sigma - \mathcal{S}_0) \tag{12}$$

where two quantities only control the frequencies ($\Re(f_{CW})$ and $\Re(f_{ACW})$) and growth rates ($\Im(f_{CW})$ and $\Im(f_{ACW})$) of the two azimuthal modes:

- the coupling strength Σ, which is the sum of all coupling parameters:

$$\Sigma = \Sigma_{i=1}^{N}\Gamma_i = \frac{\rho^0 c^0}{2S_c\rho_u^0 c_u^0} \times \Sigma_{i=1}^{N}\left[S_i tan(k_u L_i)\left(1 + n_i e^{j\omega\tau_i}\right)\right] \tag{13}$$

  The coupling strength does not depend on the pattern used to distribute burners along the azimuthal direction.
- the splitting strength $\mathcal{S}_0$, which determines the frequency split between the two modes f_{CW} and f_{ACW}. It is a function of the coupling parameters Γ_i of the N burners and (unlike Σ) of the pattern used to distribute burners along the azimuthal direction:

$$\mathcal{S}_0^2 = \Sigma_0^2 - A = \sum_{i,j=1}^{N}\Gamma_i^0\Gamma_j^0\cos\left(\frac{4p\pi}{N}(j-i)\right) = \gamma(2p)\times\gamma(-2p) \tag{14}$$

  where $\gamma(k) = \sum_{i=1}^{N}\Gamma_i^0 e^{-j2k\pi i/N}$ is the kth Fourier coefficient of the coupling factor associated with the azimuthal distribution Γ^0 and p is the mode order (usually only the first azimuthal mode $p = 1$ is observed). If all burners are identical, the splitting strength $\mathcal{S}_0$ is 0, and the two azimuthal modes have identical frequencies and growth rates.

Eqs.(12) –((14)) can then be used to analyze the stability of any annular chamber as soon as its dimensions, temperatures and FTFs are known. The next section provides an example of application of these equations to passive control using symmetry breaking.

3.3. *Passive control of azimuthal instability modes using symmetry breaking*

One attractive method to mitigate azimuthal combustion instabilities is to avoid using burners that are identical [33]. This is also called symmetry breaking. It is a well known method to avoid instabilities in many systems (one of the reasons for not having army walking over a bridge at the same pace in the field of structural mechanics). For an annular chamber, this means using burners that have different n_i's and τ_i's. There is clearly a wide range of choices if one tries to have 'different' burner types in the same engine. For the moment, most tests have been performed using only two different burner types: Siemens engines, for example, sometimes have two types of burners in the same machine. Moeck et al [57] demonstrated active control in an annular chamber where flames were replaced by electrically driven heating grids and showed that they could damp azimuthal modes by breaking symmetries (in this case, this meant using different electrical power in each sector).

To elucidate how symmetry breaking affects azimuthal modes, LES or 3D TA codes are not the best tools: a guide is needed to understand the physics before trying to simulate these mechanisms in details. Here Eqs. (12)–(14) provide a good example of the power of analytical approaches. The frequency of the clockwise mode (Eq. (12)) is $f_{CW} = \frac{c_c}{2L_c} - \frac{c_c}{4\pi L_c}(\Sigma + \mathcal{S}_0)$. The first contribution to f_{CW} is $\frac{c_c}{2L_c}$, which is the frequency of the first azimuthal mode in the chamber without active flames. The effect of the active flames is explicitly revealed in the following correction term $\Sigma + \mathcal{S}_0$: active flames act collectively to increase the coupling strength Σ independently of their positions. However, if burn-

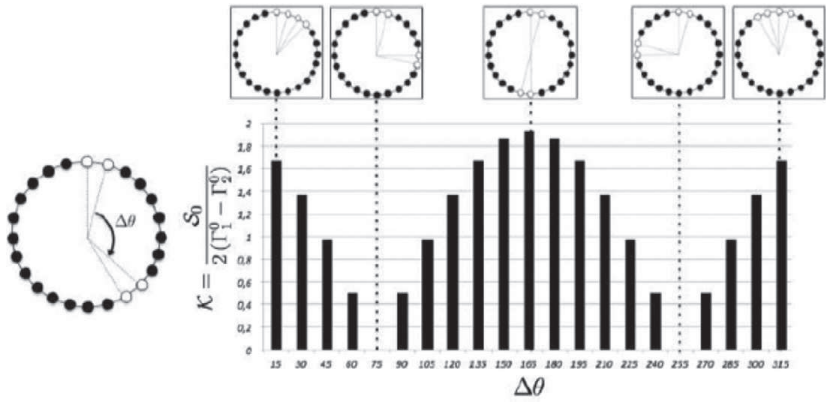

Fig. 9. Analytical analysis of symmetry breaking in a 24 burners chamber. Evolution of the splitting pattern factor $\mathcal{K}$ as a function of the angle $\Delta\Theta$ separating groups of twin type 2 burners when 4 type 2 burners are mixed with 20 type 1 burners.

ers are different, their distribution along θ matters and is measured by the splitting strength $\mathcal{S}_0$.

Eq. (12) also provides a remarkable result: it shows that splitting modes (increasing the splitting strength $\mathcal{S}_0$) is usually detrimental for stability. The imaginary parts of f_{CW} and f_{ACW} (the growth rates of the two modes) are modified by the imaginary part of the splitting strength $\mathcal{S}_0$ in opposite ways: if one of them becomes more stable, the other one becomes more unstable. This has been observed in other studies for annular chambers [57,103] but also in other fields of physics [104,105]. Therefore, it may be safer to try to mitigate azimuthal modes by changing the coupling strength Σ rather than the splitting strength [103].

If only two burner types are used (with coupling factors Γ_1 and Γ_2), this analysis can be extended because the expression of $\mathcal{S}_0$ becomes:

$$\mathcal{S}_0 = \overbrace{2\mathcal{K}}^{\text{Splitting pattern}} \cdot \underbrace{(\Gamma_1 - \Gamma_2)}_{\text{Burner difference}} \tag{15}$$

where the reduced splitting strength $\mathcal{S}_0$ depends only on $\mathcal{K}$, called a splitting pattern factor and on $(\Gamma_1 - \Gamma_2)$, which is fixed by the difference between the two burner types coupling factors.

Eq. (15) allows us to predict whether modes will split or not, and whether the resulting modes will be stable or not. It also provides a guide to place burners along the circumferential direction, in order to maximize damping or avoid splitting. For example, the distribution of four Type 2 burners with 20 Type 1 burners in a 24 sector machine can be done in many ways (Fig. 9): if the four burners of type 2 are grouped two by two, the only parameter controlling the pattern is the angle $\Delta\Theta$ between the two groups of type 2 burners. Eq. (15) gives the value of the splitting pattern factor $\mathcal{K}$ and shows that certain patterns (like those obtained for $\Delta\Theta = 75°$ or 255°) lead to a system where symmetry is broken but the mode still is degenerate ($\mathcal{K} = 0$). On the contrary, some patterns like $\Delta\Theta = 165°$, where the two pairs of burners are located on opposite sides of the chamber, maximize the splitting strength and will promote instability.

4. Recent progress on mechanisms controlling instabilities

The last 10 years have revealed that multiple mechanisms had to be taken into account to analyze instabilities in real engines. The following sections present recent results on the effects on CI of wall temperatures (Section 4.1), on the existence of intrinsic CI mode that are not controlled by the eigenmode of the chamber (Section 4.2), on the importance and determination of impedances (Section 4.3), on hydrodynamic stability results (Section 4.4) and on the links between bifurcations and CIs (Section 4.5).

4.1. The effects of wall temperatures

The temperatures of a combustor's wall can modify thermoacoustic instabilities in different ways:

- Walls cool down the burnt gases, decreasing their temperature and therefore the local sound speed. As a consequence, the eigenmodes of the chamber can change and their stability too. Adiabatic and non- adiabatic configurations exhibit different stability regions: this is easily observed in simulations where changing the wall heat transfer condition from adiabatic to isothermal is sufficient to trigger or damp modes [106,107]. This is a rather obvious effect due to changes in sound speeds and flame shapes which will not be discussed here.
- Heat losses in the zones that are critical for flame stabilization play a more interesting role. Since these regions (flame holders for example) control the flame roots, they

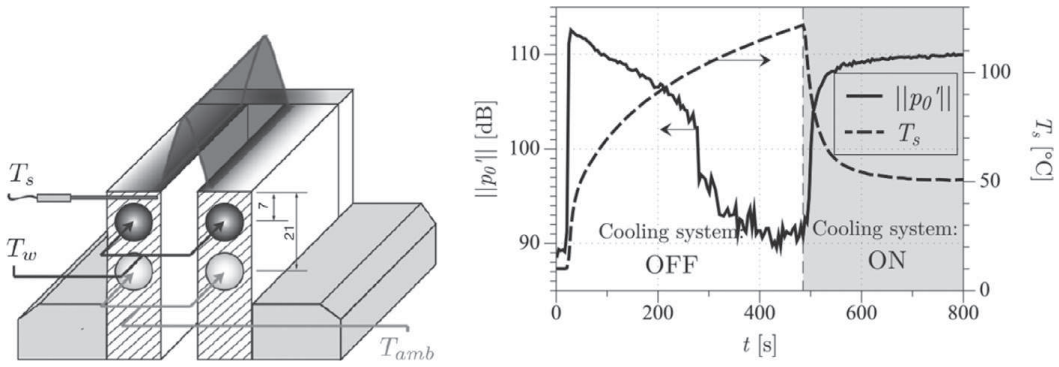

Fig. 10. Demonstrating the effects of flame holder temperature on the stability of a laminar premixed Bunsen flame [113]. Left: a Bunsen flame stabilized on a water-cooled slot. Right: evolution of pressure oscillations and slot wall temperature versus time. The cooling system is started at t =490 s.

also affect its response to perturbations [73]. This point is discussed here because it is often ignored in simulation tools (Fig. 4) even though recent studies prove that it can be a critical issue.

It is well-known that heat losses introduced by flame-holders or by walls close to the stabilization zone of flames induce strong changes on the flame topology even in the absence of any instability [37,108]. For porous burners, the whole stabilization process and the flame response to unstable perturbations is controlled by heat losses to the porous plate [109–111]. Even for usual Bunsen burners, the temperature of the lateral walls [8,112] plays a major role on flame stabilization. Therefore, it is not surprising that instabilities are also affected by the temperature field of the solid on which a flame is anchored: an example of wall temperature effects on combustion instabilities was given by Mejia et al. [113] who showed that the self-excited mode of a laminar premixed flame stabilized on a slot was directly controlled by the slot wall temperature. This metal temperature was controlled by liquid cooling and measured by a thermocouple. When the experiment is ignited, walls are cold and the instability begins right away at a high level (110 dB). The wall temperature increases slowly and when it does, the pressure oscillations decrease. After 300 s, the walls are warm (close to 120 °C) and the instability has completely disappeared. At 490 s, the liquid cooling system is activated: the wall temperature goes down again and the instability goes back to its initial level. This demonstrates that the temperature of the wall plays a strong role in the determination of the stability characteristics of this flame.

Why the flame-holder temperature changes the stability of a combustor is not discussed often. In most models, the flame-holders are supposed to be adiabatic and the flame is anchored on the flame holder itself. This allows a theoretical analysis of the flame response to forcing using G-equation formulations as proposed by Boyer and Quinard [114] and by others [115]. In these first approaches, the flame front was supposed to be perfectly anchored to the flame holder and unable to move. The first authors who mentioned that the point where the flame is stabilized (the flame root) also moves and can affect the flame FTF, were Lee and Lieuwen [116] who proposed to separate the dynamics and therefore the FTF of an anchored flame into two contributions:

- flame front contribution (the movements of the flame when it is perturbed: this is an essentially kinematic mechanism that can be predicted with tools such as the G-equation)
- flame root contribution (the movements of the point where the flame anchors when it is perturbed, which requires to solve the near-wall region where the flame touches the wall).

While the first contribution has been studied by many authors, the second contribution due to flame root movements remains the weak part of this approach because it required solving for the temperature field in both gas and solid. Following the analysis of Rook et al. [117] (for flat flames), Cuquel et al. [9] derived a full model for anchored flames accounting for both flame root and flame front dynamics. Fig. 11 illustrates these two mechanisms and shows how the stand-off distance between flame holder and flame root was estimated experimentally by Mejia et al. [113] from a direct view of light emission in a slot stabilized premixed flame.

When the flame is submitted to acoustic fluctuations (for example to estimate its FTF), perturbations propagate along the flame front (flame front contribution) but the flame root moves too (flame root contribution). The movement of the flame during an oscillation cycle is displayed in Fig. 12 (left) while the movement of the flame root (marked by a cross) is displayed in Fig. 12 right.

Mejia et al. [113] showed that accounting for the flame root dynamics allowed to explain the effects of the wall temperature on the flame stability: it

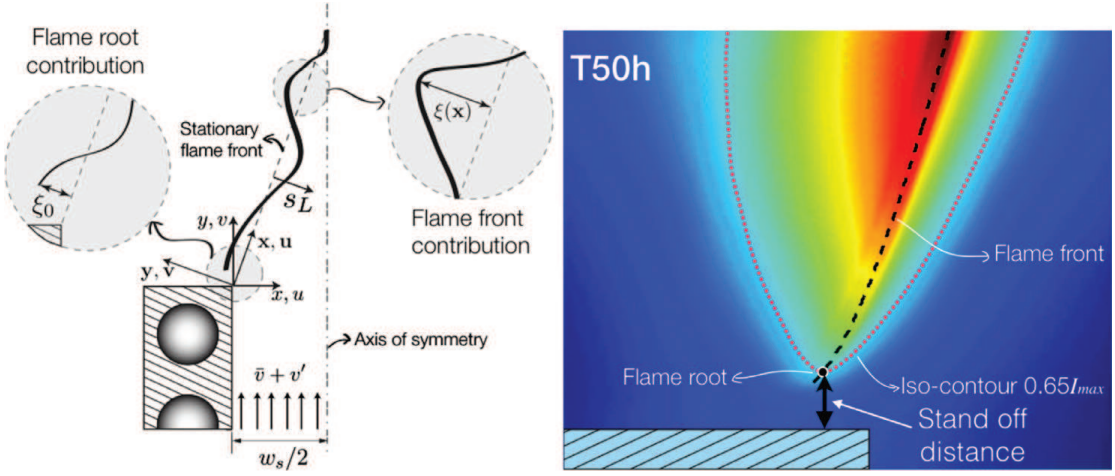

Fig. 11. Left: the two mechanisms contributing to the FTF of an inverted V-flame stabilized on a slot (from [9,113]). Right: visualization of the stand-off distance between flame holder and flame root [113].

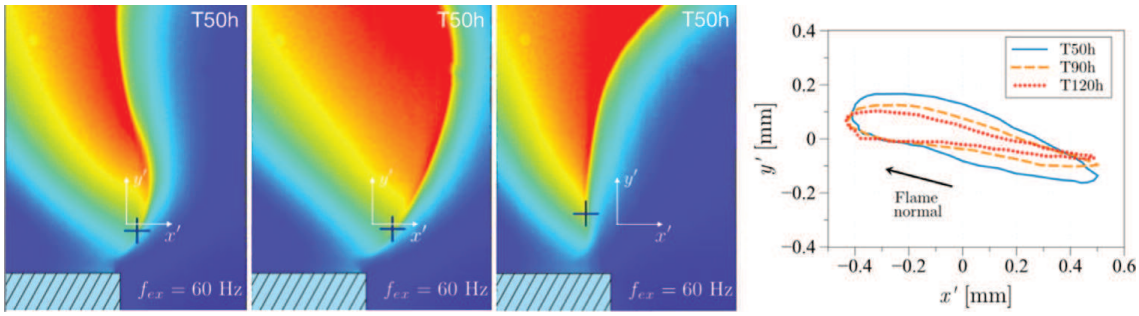

Fig. 12. Left: visualization of the flame movements for an inverted V-flame submitted to a 60 Hz forcing with a flame holder temperature of 50 °C. The + symbol marks the flame root and the trajectories of the flame root are displayed for three different temperatures of the flame holder (50, 90 and 150 °C) [113].

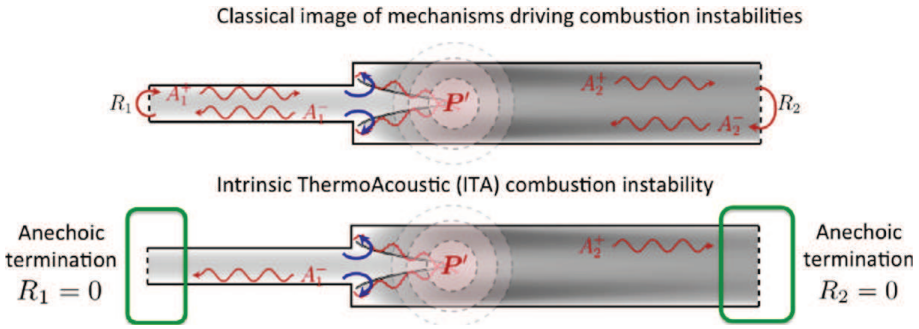

Fig. 13. Top: the classical paradigm for combustion instabilities (a resonance between the flame and the acoustic eigenmodes of the chamber reflecting on its inlet and outlet). Bottom: (ITA) intrinsic thermoacoustic modes (a resonant mode that does not involve any acoustic eigenmode of the chamber).

modifies the FTF sufficiently to transform a stable into an unstable flame (and vice versa) and explains the observations of Fig. 10.

4.2. *Intrinsic acoustic modes*

The general picture used to study and mitigate combustion instabilities today (Fig. 13) links oscillations of heat release with acoustic eigenmodes of the combustion chamber as introduced for the model of Fig. 2. These eigenmodes are due (for longitudinal oscillations) to acoustic reflections at the inlet and outlet characterized by their respective reflection coefficients R_1 and R_2. This view has many direct implications for the analysis of instabilities:

- When a combustor is unstable, the usual procedure is to compute the acoustic modes of the chamber and check whether the

frequency of the instability matches one of the eigenmodes frequencies.
- To stabilize the mode, increasing acoustic losses at inlet and outlet is the usual route: diminishing R_1 and R_2 is supposed to diminish the growth rate of the modes by increasing losses.

In 2014, the TU Munich and the Eindhoven groups [118,119] indicated that another mechanism may be found in flames: intrinsic thermoacoustic (ITA) modes. The theory for ITA modes is simple and starts from the following question: what would happen in the flame of Fig. 2 if both extremities would be perfectly anechoic (Fig. 13)? According to the classical paradigm for CI, such a system would have no acoustic eigenmode and a maximum level of acoustic loss: any perturbation created by the flame and propagating toward inlet or outlet would simply leave, thereby eliminating possible resonances with the flame. Therefore the two acoustic waves A_1^+ and A_2^- would be zero. In practice, this is not exactly what theory says. Starting from the equations of the toy model (Eq. (3)) and using $A_1^+ = A_2^- = 0$ does not lead to an impossible solution but to :

$$p'_2(x=0,t) = p'_1(x=0,t) \text{ so that}$$
$$A_2^+ + \cancel{A_2^-} = \cancel{A_1^+} + A_1^- \tag{16}$$

and

$$S_2 u'_2(x=0,t) = S_1 u'_1(x=0,t) + \frac{\gamma-1}{\rho_1 c_1^2}\dot{\Omega}' \tag{17}$$

so that:

$$A_2^+ - \cancel{A_2^-} = \Gamma\left(\cancel{A_1^+} - A_1^-\right)(1+\theta F(\omega)) \tag{18}$$

where $\Gamma = \frac{\rho_2 c_2}{\rho_1 c_1}\frac{S_1}{S_2}$ and the general expression $\theta F(\omega)$ has been used to replace $ne^{j\omega\tau}$ in the Crocco equation. The θ factor ($\theta = T_2/T_1 - 1$) corresponds to the low-frequency value of the FTF and provides a proper scaling for $F(\omega)$. Eq. (18) has a solution when:

$$1 + \Gamma[1+\theta F(\omega)] = 0 \text{ or } \theta \mathrm{F}(\omega) = -\frac{1+\Gamma}{\Gamma} \tag{19}$$

where $\theta = \frac{T_2}{T_1} - 1$. The solutions of Eq. (19) are a set of modes of pulsation ω that must satisfy:

$$\begin{cases} \arg\left(F(\omega)\right) = (2q-1)\pi \quad (q \in \mathbb{N}^*) \\ |F(\omega)| = \dfrac{\Gamma+1}{\theta\Gamma} \end{cases} \tag{20}$$

When the usual Crocco expression is used for the FTF $F(\omega)$: $\theta F(\omega) = ne^{j\omega\tau}$, Eq. (20) has an explicit solution:

$$\begin{cases} \omega_r = \dfrac{(2q-1)\pi}{\tau} \\ \omega_i = \dfrac{1}{\tau}\ln\left(\dfrac{n\Gamma}{1+\Gamma}\right) \end{cases} \tag{21}$$

where q ($q \geq 1$) is an integer giving the mode order. The first ITA mode ($q = 1$) has a real pulsation $\omega_r = \frac{\pi}{\tau}$ and a period $T = 2\tau$. It is amplified if ω_i is positive which is the case when $n \geq n_c = \frac{1+\Gamma}{\Gamma}$ or, in terms of the modulus of the FTF $F(\omega)$: $F \geq F_c = \frac{1+\Gamma}{\theta\Gamma}$.

This first ITA mode is very different from usual thermoacoustic modes:

- Its stability is not controlled by the time delay τ (as it was for the toy model: see Eq. (8)) but rather by the FTF gain n, i.e. by the strength of the flame response to acoustic perturbation.
- Its period T is not linked to any acoustic period of the combustor (that has no eigenfrequency in any case because it is terminated by anechoic sections on both sides). T is simply equal to two times the flame delay τ.

ITA modes have two additional properties: (1) they react to changes in boundary conditions differently from usual thermoacoustic modes and (2) they can interact with usual thermoacoustic modes. For example, adding acoustic dissipation at inlet and outlet in a burner can make ITA modes more unstable, a property that is totally unexpected for classical acoustic modes. Hoeijmakers et al. [118] show for example a map of the modes location in the (ω_i, ω_r) plane for a toy model similar to Fig. 2. They use two cases: on the left of Fig. 14, for a case where the ITA mode is stable ($F \leq F_c$), there is an unstable standing mode when $R_1 = 1$ and $R_2 = -1$. When the reflection coefficients of inlet and/or outlet decrease, this mode becomes more stable and when $R_1 = R_2 = 0$, the system reaches the condition where the ITA mode may appear. Since the mode is stable, it does not appear and the system behaves as expected: making the inlet and outlet anechoic drives the system to stability. On the other hand, if the ITA mode is unstable ($F \geq F_c$, right image in Fig. 14), the standing mode that is unstable when $R_1 = 1$ and $R_2 = -1$ becomes an unstable ITA mode when R_1 and R_2 vanish. In this situation, making inlet and outlet anechoic does not stabilize the system: it transforms the initially unstable standing mode into an unstable ITA mode.

The ITA instability criterion $F \geq F_c = \frac{1+\Gamma}{\theta\Gamma}$ can be explicited for a perfect gas with constant molecular weight where $\Gamma = \frac{\rho_2 c_2}{\rho_1 c_1}\frac{S_1}{S_2} = \sqrt{\frac{T_1}{T_2}}\frac{S_1}{S_2}$, knowing that $\theta = \frac{T_2}{T_1} - 1$:

$$F \geq F_c = \frac{1+\Gamma}{\theta\Gamma} = \frac{1}{T_2/T_1 - 1}\left(1 + \frac{S_2}{S_1}\sqrt{\frac{T_1}{T_2}}\right) \tag{22}$$

In most flames the maximum values of the FTF gain F are known and are of order unity. ITA modes will appear if the critical threshold F_c becomes less than F. Eq. (22) shows that the ITA critical threshold F_c goes down when the section ratio between inlet duct and combustion chamber goes

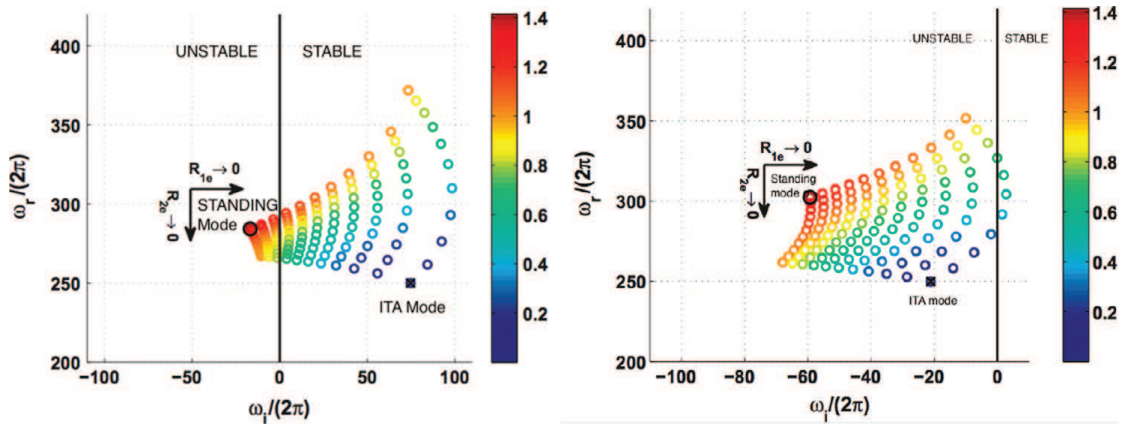

Fig. 14. Example of trajectories of ITA modes for a toy model similar to Fig. 2 when the reflection coefficients of the inlet and outlet vary (from Hoeijmakers et al. [118]). Left: stable ITA mode ($F \leq F_c$). Right : unstable ITA mode ($F \geq F_c$). The color scale corresponds to the value of $\sqrt{R_1^2 + R_2^2}$ and measures the separation from a perfectly anechoic system.

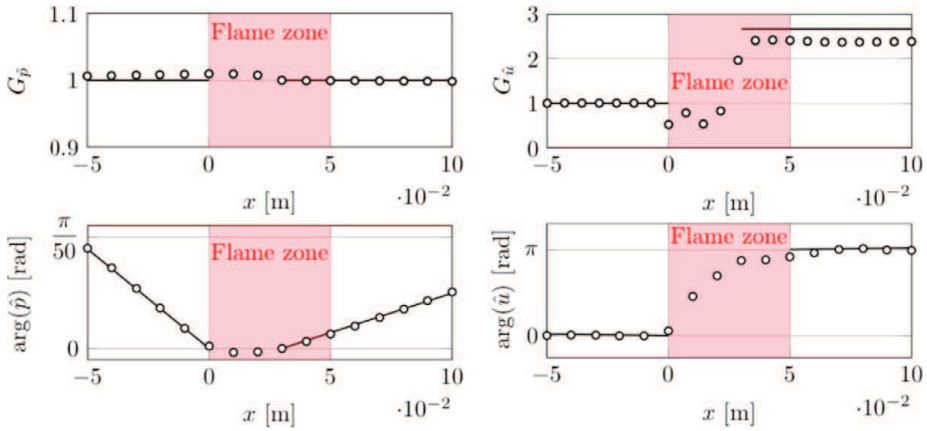

Fig. 15. First ITA mode structure for the configuration of Fig. 2 [120]. Solid line: theory (Eq. (23)). Symbols: DNS.

down (S_2/S_1 decreasing) or when the temperature ratio goes up (T_2/T_1 increasing): intense flames in chambers with small section changes (strong confinement) should be more prone to intrinsic instabilities. This may explain why ITA instabilities have not been observed very often up to now: they are triggered when the power per unit volume goes up (high values of T_2/T_1) or when the chambers volume diminishes. Since both effects are sought in future engines, ITA might appear in real engines soon. Their study and control will require to think differently compared to today's state of the art: for example, ITA modes will respond in unexpected ways to increased acoustic losses that will make ITA modes even more unstable. A whole field of research is probably opening up in this domain.

The exact mechanisms that trigger the unstable loop of ITA modes without feeding the acoustic chamber modes are not fully clear yet. Courtine et al. [58] used DNS of ITA modes in a laminar flame similar to Fig. 2. They studied various confinements (S_2/S_1 from 1.5 to 6) and showed that, as expected, the smallest confinement ratios lead to unstable ITA modes. Fig. 15 shows the pressure and velocity fluctuations (modulus and phase) obtained by theory (solid lines) and by DNS. The structure of the first ITA mode can be obtained by injecting the ω expression (Eq. (21)) into Eq. (1) leading to:

$$\frac{|\hat{p}_2|}{|\hat{p}_1|} = 1 \quad \text{and} \quad \frac{|\hat{u}_2|}{|\hat{u}_1|} = \frac{S_1}{S_2}(\theta|F| - 1) \tag{23}$$

for modulus and:

$$\begin{aligned} \arg[\hat{p}_1] &= -\frac{\pi}{c_1\tau}x \quad \arg[\hat{p}_2] = \frac{\pi}{c_2\tau}x \\ \arg[\hat{u}_1] &= -\frac{\pi}{c_1\tau}x \quad \arg[\hat{u}_2] = \frac{\pi}{c_2\tau}x + \pi \end{aligned} \tag{24}$$

for phases.

The agreement between theory (Eq. (23)) and DNS is very good and confirms the expected nature of the mode. Only acoustic propagation is observed downstream or upstream of the flame zone: the phase unwraps at the sound speeds on both sides of the flame and the unsteady pressure is the same everywhere, showing that the flame is the acoustic source and that waves propagate from the flame zone without any reflection. No node is observed anywhere. The jump in unsteady velocity between

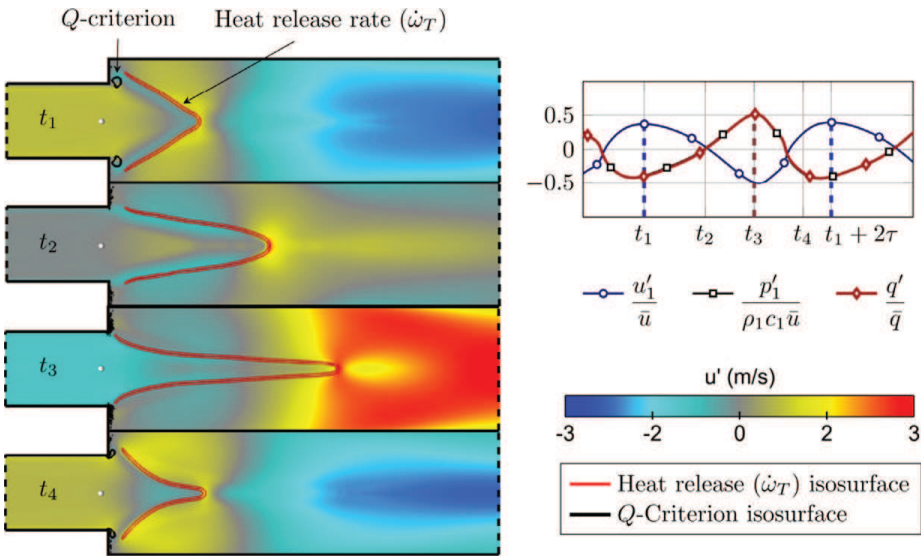

Fig. 16. Unstable loop driving the first ITA mode of Fig. 2 [58].

the cold and the burnt gases $\frac{S_1}{S_2}(\theta|F|-1)$ is also well captured even if hydrodynamic mechanisms in the flame zone induce unsteady velocities that cannot be captured by theory.

The mechanisms controlling ITA modes are obviously present in the DNS but they also are contained in the FTF formulation used for theory. The FTF assumes velocity-sensitive flames: the flame is modified when the inlet velocity of the chamber is changing. For ITA modes, this concept becomes a little bit more difficult to understand because there is no downstream acoustic wave entering the burner of Fig. 2 through the inlet which is anechoic. Still, the flame oscillate. This point has been discussed in the literature and is still an open question [58,119,120].

Independently of the FTF formulation necessary to capture ITA modes, the mechanisms controlling the mode can be isolated from the DNS. Fig. 16 displays four snapshots of the flow during one unstable cycle (left) and the time evolution of chamber pressure, reference point velocity (in inlet duct) and total heat release. All time signals are strongly non linear, even pressure, something unusual in most usual thermoacoustic instability. The chamber pressure and the reference point velocity are perfectly out of phase as expected from Crocco's relation Eq. (4) when the period of the mode is twice the flame delay τ. Since the chamber pressure and the reference velocity are also out of phase (Fig. 15), the heat release and the chamber pressure are in phase as expected from the Rayleigh criterion. The left part of Fig. 16 shows that the cycle begins when a vortical perturbation (visualized by the Q criterion [121]) is initiated at the corners of the dump plane (instant t_1). This vortical perturbation travels along the flame front and increases its surface (time t_2). At instant t_3, the flame reaches its maximum length and heat release is maximum too. At this time the velocity in the inlet duct is minimum and the flame has to retract very rapidly toward the dump plane by the usual flame restoration mechanism. This creates an acoustic wave propagating upstream and impinging on the corner. At this instant (time t_4), mode conversion takes place at the corner, transforming the acoustic wave into a new vortical wave and closing the cycle. Mode conversion [122] is an important part of the unstable loop: it transforms acoustic waves into vorticity at the corners of the dump plane. All mechanisms take place between the dump plane and the extreme position of the flame: downstream convection of the vortical wave created by mode conversion at the dump plane followed by a fast acoustic propagation leading to a new mode conversion. No acoustic reflection from the chamber inlet or outlet is involved: this was also verified by Courtine [58] by performing the same simulation in a chamber where the lengths of inlet and combustion chamber were multiplied by two, leading to exactly the same mode.

Most studies on ITA modes have been theoretical [119] or numerical [58] but up to now, experimental work has been limited to the PhD work of Hoeijmakers in Eindhoven. To construct a setup exhibiting an ITA mode, the difficulty is that inlet and outlet must both be as anechoic as possible to ensure that $R_1 = R_2 = 0$. This can be obtained by installing horns on inlet and outlet ducts but doing so perfectly is arduous especially on the exhaust side where hot gases leave the chamber and a heat exchanger is required to protect the exhaust duct. Fig. 17 shows the experiment of Hoeijmakers, including a large horn at the flow inlet and a set of laminar premixed flames in the chamber. ITA modes renew the classical view of thermoacoustic modes in a combustion chamber when only one loop was present : the flame creates noise which is reflected back to the flame. This classical

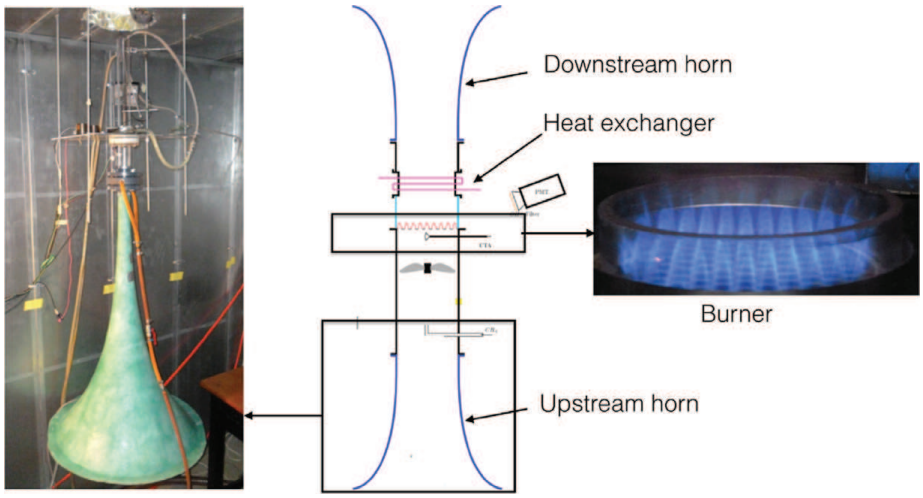

Fig. 17. Experimental configuration to study ITA modes for laminar flames (PhD of P.G.M. Hoeijmakers, 2014).

interpretation ignores ITA modes which are due to a resonant loop within the flame zone itself: in practice, thermoacoustics in a combustion chamber involves two different loops, one associated to the flame itself, controlled by the FTF, and another one controlled by the geometry of the combustor, in particular its inlet/outlet reflection coefficients. ITA modes (observed for zero reflection coefficients) and cavity modes (observed without active flame) are decoupled. However, as soon as these two loops start interacting (with non-null reflection coefficients and an active flame), they perturb both cavity modes and ITA modes, making them potentially unstable. Perturbed cavity modes are the classical thermoacoustic modes, while perturbed ITA modes are still to be studied. How these two types of modes interact in a real configuration is an open topic today.

4.3. Impedances

As suggested by the analysis of Section 2.1, all combustion instabilities are controlled by the acoustic behavior of the inlet and outlet of the combustion chamber: the impedances (or the reflection coefficients) at the chamber extremities affect directly the frequency and the growth rates of all modes. The notion of impedance is the simplest approach (in the linear regime) to characterize wave transmission and reflection at a given section (usually at the inlet and outlet of the combustion chamber). The effect of all parts located downstream of this section are lumped in an impedance Z defined by:

$$Z = \frac{1}{\bar{\rho} c} \frac{\hat{p}}{\hat{u}} \tag{25}$$

Impedances are complex numbers varying with frequency. They can also be expressed in terms of reflection coefficients R: at an outlet, using the notations of Eq. (1), the reflection coefficient R measures the ratio of the acoustic wave entering the domain A^- to the wave leaving it, A^+. Reflection coefficients depend on a given axis orientation (to decide which wave is the incident and which one is the reflected one): for example, if R is defined as A^-/A^+, Z is simply given by: $R = (Z+1)/(Z-1)$. Knowing Z or R (as a function of frequency) at the inlet or outlet of a combustion chamber is sufficient to study its stability in the linear domain. For longitudinal waves, Z fully describes all relevant mechanisms taking place outside of the chamber.

The need to integrate impedances into any analysis of combustion instabilities has many implications:

- The stability of an isolated combustion chamber has no real meaning: the stability of a chamber depends on its own characteristics but also on the impedances imposed on all its inlets and outlets. The same chamber tested in a given bench will behave in a different way when installed on the real engine for example. This explains why studying instabilities can become complicated: extracting a chamber from an unstable engine to study it in the laboratory (with different impedances) will lead to different results. Vice versa, struggling to stabilize a chamber on a laboratory bench might be detrimental to the stability of the real engine.
- The only meaningful approach to combustion instabilities is therefore to integrate the impedances of inlets and outlets into the analysis, considering them as input data controlling stability like equivalence ratio, total flow rate or geometry. Here combustion systems can be split into two categories: (1) systems where impedances are known or can be determined reasonably well and (2) systems where impedances are very difficult to evaluate, for example gas turbines where the inlet

Table 1
Impedances (Z) of one-dimensional ducts.

Case	Configuration	Boundary condition	Impedance $Z = \frac{1}{\bar{\rho}c}\frac{p'}{u'}$
Outlet	1/ Infinite duct	Non reflecting	1
Inlet	2/ Infinite duct	Non reflecting	-1
Outlet	3/ Constant pressure	$p' = 0$	0
Inlet	4/ Wall	$u' = 0$	∞
Inlet	5/ Choked nozzle	$u' = 0$	∞
Outlet	6/ Choked nozzle	$u' = 0$	∞

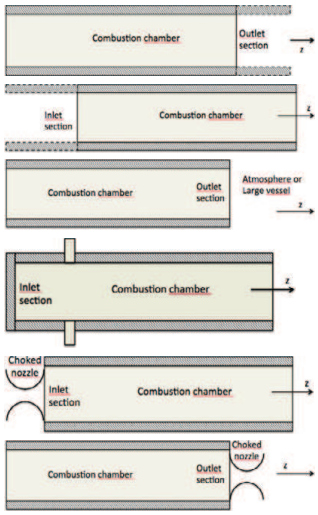

of the chamber corresponds to the outlet of a compressor and the chamber outlet is the turbine inlet. Determining the impedances of turbomachinery systems is still an open research question today.

4.3.1. *The impedances of laboratory rigs*

Inlets and outlets ducts in laboratory experiments used for CIs studies are normally designed to provide simple impedances (Tab. 1). Outlets for example often correspond to a duct terminating into open atmosphere (case 3 in Tab. 1). A few other cases are relevant for combustion chambers installed in laboratories. Motheau et al. [123,124] showed that a choked nozzle at the inlet of a chamber (Case 5) imposes a constant inlet velocity ($u' = 0$). When the chamber is terminated by a choked nozzle, the simplest acoustic approximation [125] is to replace it by a wall (Case 6). This low-frequency evaluation can be replaced by more sophisticated approaches when the nozzle cannot be considered as compact compared to the acoustic wavelength [126,127].

In real engines, Tab. 1 is rarely useful and more complex impedances are required. In a gas turbine, the only simple case is a choked chamber outlet which can be approximated by $u' = 0$ to first order (Case 6). In a rocket engine, terminated by a large nozzle, this may also be an acceptable approximation.

For CIs, knowing impedances is critical but manipulating inlet and outlet impedances can also be useful: modifying impedances on any side of combustion chamber is a well-known method to mitigate combustion instabilities in academic systems. Active control as developed in the 80s can be viewed as such a technique [78,128,129]. Passive systems can also be added, for example at the chamber inlet, to control its impedance [130,131] either to damp a given CI mode or to reinforce it (Fig. 18). These studies confirm the importance of inlet and outlet impedances to predict CIs. This is a major difficulty in real systems as shown in the next section.

4.3.2. *The impedances of compressors and turbines*

In gas turbines, the presence of a compressor and a turbine raises a new and unexpected difficulty to predict CIs. The impedances of these turbomachinery systems control the acoustic modes of the whole system and are required to predict CIs but unfortunately they are usually unknown and difficult to measure. Only turbine companies and a few laboratories in the world can build benches where the impedance of a compressor or of a turbine can be measured with precision. In addition, compressors and turbines are not passive acoustic elements: they can inject unsteady energy into the chamber on a number of frequencies, thereby exciting the combustion process itself.

The question of turbomachinery impedances needed to study CIs has many common aspects with the problem of combustion noise [132,133] and especially of noise transmission and generation through turbine stages [126,134–140]. This problem has been studied in details over the last 10 years as combustion noise has progressively become a significant part of the overall noise of aircraft and helicopters because the other sources of noise (jet noise, fan noise) have decreased. To predict combustion noise (Fig. 19), it is necessary to build a model describing how much acoustic energy is transported from the chamber to the atmosphere through the turbine stages. This task is almost the same as predicting how much of this

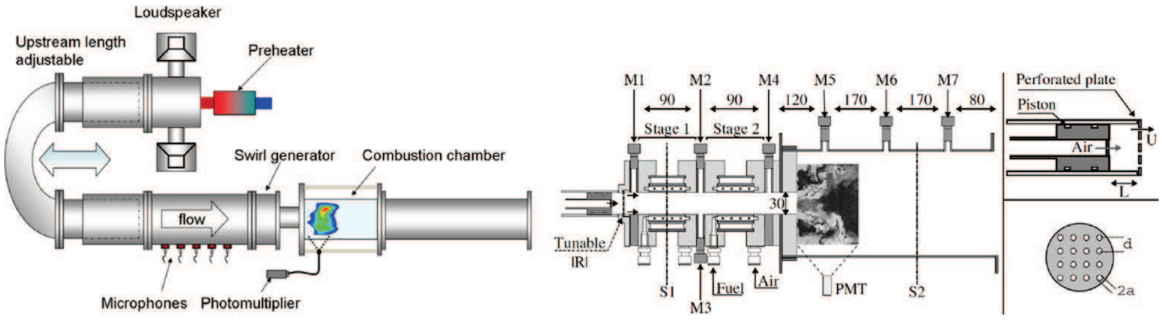

Fig. 18. Examples of systems to adjust inlet impedances: left, a variable length inlet duct used by Cosic et al. [131] to force transverse modes; right: a perforated plate with adjustable bias flow by Tran et al. [130] to inhibit modes.

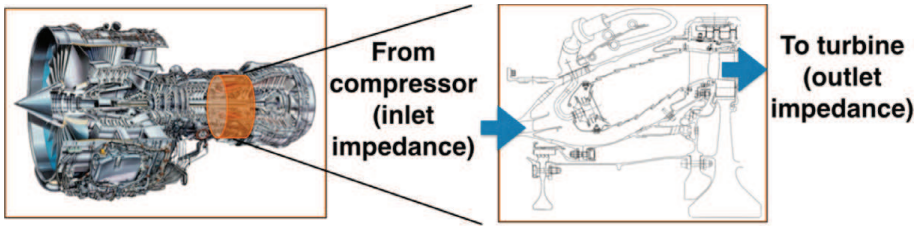

Fig. 19. A combustion chamber in a gas turbine with impedances on inlet (compressor) and outlet (turbine).

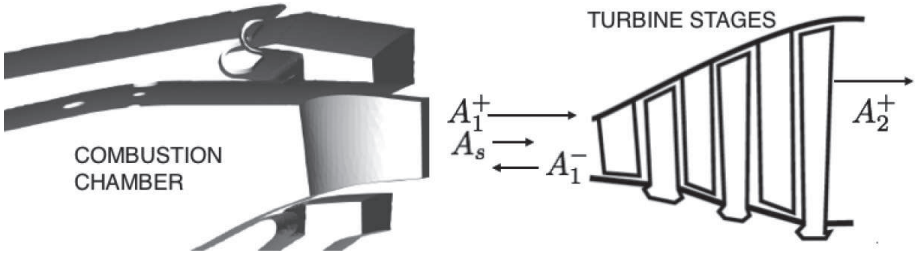

Fig. 20. Transmission of acoustic (A_1^+) and entropy (A_s) waves through the turbine: the transmitted acoustic wave (A_2^+) is the combustion noise; the reflected acoustic wave (A_1^-) can excite mixed modes in the chamber.

energy is actually reflected back into the chamber, an information directly linked to the impedance needed for CI studies.

The calculation of impedances of turbine (or of compressors using the same methodology) can be performed with various levels of complexity. The impedance of a nozzle can be computed using compact theories [138,141] (where the wavelength of the acoustic waves is supposed to be large compared to the nozzle axial dimension) or, more recently, new analytical theories [126,127] that provide nozzle impedances at all frequencies corresponding to longitudinal modes. A simple area contraction however is a poor model for what is taking place in a real turbine stage where strong flow deviations are created by vanes. Moreover, all rotor stages also introduce enthalpy jumps. Cumpsty and Marble [134,142] were the first to propose models to describe the impedances of stator stages in the low-frequency limit ('disk actuator' theory). These studies were motivated by indirect noise, a mechanism that transforms hot spots (generated within the chamber: A_s in Fig. 20) into acoustic noise (A_2^+) when the entropy waves are accelerated within the turbine stages. To describe how entropy and acoustic waves interact and propagate within turbo machinery stages, the disk actuator theory assumes that the stage is compact: jump conditions, rigorously valid at zero frequencies, are used to link incident and transmitted waves. By assembling jump conditions for rotor and stator stages, the impedance of a full turbine or of a compressor can be obtained [143,144].

4.3.3. *Entropy–acoustic modes*

The transmission of entropy waves through turbine stages creates indirect noise that is propagated downstream. During the same process, the entropy waves also induce acoustic waves that are reflected back into the chamber and create a new class of CI: entropy–acoustic modes. For these modes, reflected acoustic waves (A_1^- in Fig. 20) propagate back into the combustion chamber and generate CIs that are not captured by usual thermoacoustic analysis because the acoustic field is not fed by unsteady reaction rate (as supposed in Crocco's

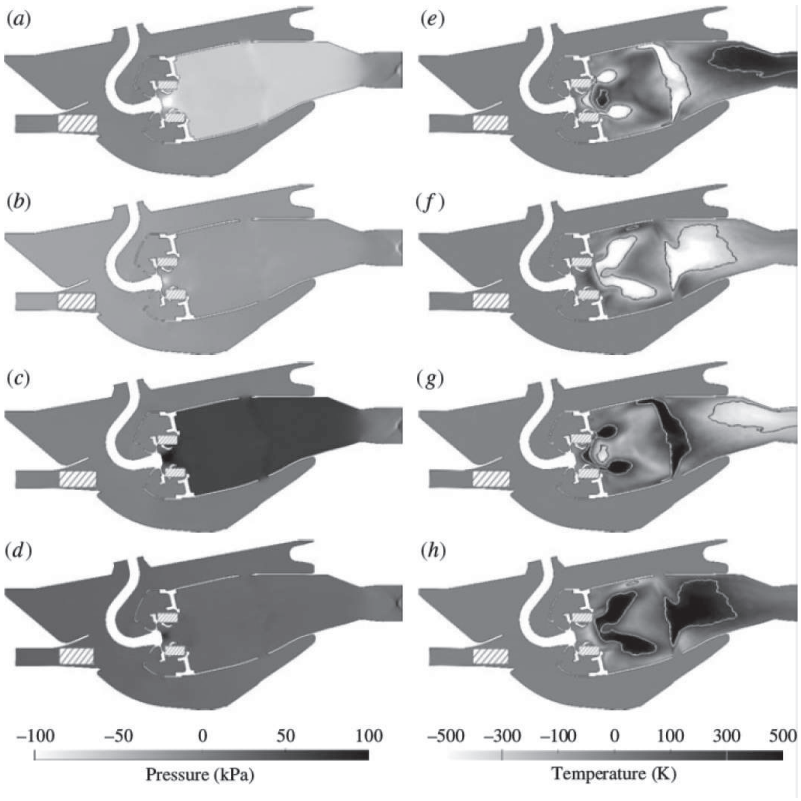

Fig. 21. A mixed mode cycle (four instants separated by $\pi/2$) in an aircraft chamber terminated by a nozzle [124]. Left: pressure fluctuations. Right: temperature fluctuations.

model, Eq. (4)) but by the acoustic reflection of entropy waves hitting the turbine. This mechanism, sometimes called mixed entropy-acoustic mode [145–147], is specific to chambers terminated by area restrictions: academic chambers terminated by a nozzle as well as real gas turbines chambers feeding turbine stages. Precise models are difficult to construct for mixed modes because entropy waves are dissipated by turbulent mixing much faster than acoustic waves in their travel from the combustion zone to the turbine. Evaluating this dissipation is complicated [148] because it depends on the flow details within the combustor [145]. Entropy waves are often dissipated too fast to feed mixed modes efficiently but this is not a general rule: for short chambers where the turbine is close to the injector, or for chambers where dilution jets can induce unsteady temperature fluctuations when they mix with burnt gases, mixed modes can be observed. For example, Motheau et al. [124] showed that a mixed mode was responsible for a strong CI at a frequency that does not match any acoustic mode of the chamber in an aircraft configuration. An unstable cycle is displayed in Fig. 21: the temperature field shows how hot pockets of burnt gases are released behind the dilution jets and propagate toward the outlet nozzle where they create an upstream acoustic wave (Fig. 22).

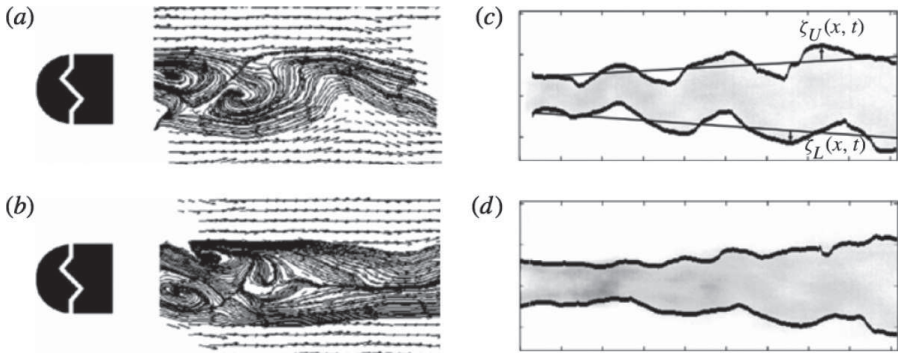

Fig. 22. Emerson et al. [149] experiment: a turbulent premixed flame is stabilized behind a bluff body for two values of the density ratio between fresh and burnt gases. Streamlines (left) and flame front position (right) for $\rho_u/\rho_b = 1.7$ (a and c) and $\rho_u/\rho_b = 2.4$ (b and d).

4.4. Hydrodynamic stability

Even though most of this review has focused on acoustic mechanisms controlling CI, purely hydrodynamic phenomena play an essential role too because they determine the flow sensitivity to acoustic forcing. Two aspects are especially relevant when discussing instabilities observed in gas turbine engines: (1) the effects of the temperature (or density) differences between fresh and burnt gases and of confinement in real engines and (2) the specific instabilities due to swirl. Both issues are critical in real engines.

4.4.1. Density ratio effects

An important difference between laboratory experiments and real engines is the temperature of the inlet gases: in laboratory systems, it is usually of the order of 300 K while it is closer to 700 K or more in real gas turbines. This increase of inlet temperature does not lead to a comparable increase on the adiabatic flame temperature because of dissociations in the burnt gases so that the burnt gas temperature remains in the range 1500–2500 K. Moreover, engines often run leaner than laboratory test rigs so that the burnt gas temperature decreases. This implies that the density ratio between fresh and burnt gases ρ_u/ρ_b which is of the order or 6–8 in laboratory flames, decreases significantly in a real engine to values smaller than 3. This observation would be of limited importance if the hydrodynamic stability of shear layers with density gradients would not vary when ρ_u/ρ_b decreases. In practice, it does change significantly and shear layers with small values of ρ_u/ρ_b exhibit additional sinuous modes that are not observed in laboratory flames. A good example of such mechanisms was given by Emerson et al. [149] using experimental data and linear stability analysis of a flame stabilized behind a bluff body where the inlet temperature could be changed (using a vitiation system) to reach values of ρ_u/ρ_b as low as 2.

Emerson's results suggest that real engines may exhibit new hydrodynamic sinuous modes compared to usual laboratory flames. Once again, this also demonstrates the difficulty of studying CIs of real engines in laboratory set-ups where the conditions are very different: using large values of the density ratio ρ_u/ρ_b may simply lead us to ignore an unstable hydrodynamic mode that is important in a real engine.

A second specificity of real engines is the strong confinement effects compared with many laboratory experiments: this leads to flows that are more unstable than unconfined flows and where absolute instabilities appear sooner [150].

4.4.2. Global stability of swirling flows

Many natural hydrodynamic modes appear in swirled flows, with and without combustion. Among all helical, shear later disturbances of swirled flows, the most well known is the PVC (precessing vortex core) and it plays a role in many CIs. Experiments [15,151–153] as well as LES [12,14,154,155] showed that PVCs can trigger certain CI modes, disappear when the flame is ignited or appear only for certain flame positions. PVCs can even appear intermittently during CI.

The exact causality link between PVC and CI remains mysterious in most cases, however. Are PVCs a source of CIs or just a second-order phenomenon ? To investigate this question, an important tool is the hydrodynamic stability analysis of swirled flows with density changes. Like Emerson [149], Terhaar et al. [16] proved that density variations play a strong role on the linear stability of a swirled flow. By forcing swirled flames using both experiments and linear stability analysis based on the mean flow profiles, Oberleithner et al. [153,156] described how the flame reacts to forcing and saturates at large amplitudes, explaining the mechanisms that lead to the variations of Flame Describing Functions with amplitude. None of these experiments corresponds to self-excited CI but results demonstrate that linear stability analysis will play a strong role in the future for CI investigations.

4.5. Hysteresis and combustion instability induced bifurcations

Most approaches for CIs view them as small perturbations imposed on a fixed mean flow. In reality, CIs can induce perturbations that are so large that the mean flow itself changes. This can occur in two ways:

- The level of perturbations can be large enough to create a pulsating flame which, if averaged over time, is quite different from the stable flame but returns to its stable state if the instability is controlled. A simple example was given in the bottom right images of Fig. 1 where mushroom-shaped vortices appear during CI but the flame returns to its stable position when the instability disappears.
- A more complex situation can be observed where a CI mode will trigger a full change of the mean flow state. This is observed in combustion systems that are prone to hysteresis mechanisms and exhibit multiple states for a fixed regime: CI induced oscillations can force the flame to transition from one state to another. Flame flashback [157,158] can be one manifestation of such an interaction between CI and mean flow.

This section discusses the second case, observed, for example, in the complex swirled flames found in gas turbines. It is well known that swirled flames can exhibit multiple stabilization states depending on small variations of geometry or of operating conditions [159]. However, even for a fixed

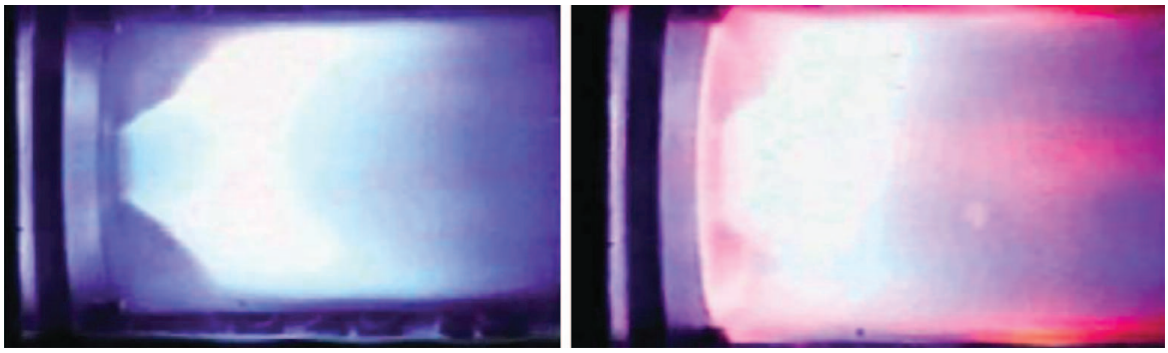

Fig. 23. State change in a swirled laboratory flame due to a variation of inlet temperature T_{in} [163]. Left ($T_{in} = 570$ K): the ORZ (outer recirculation zone) contains cold gases. Right ($T_{in} = 660$ K): the ORZ contains burnt gases.

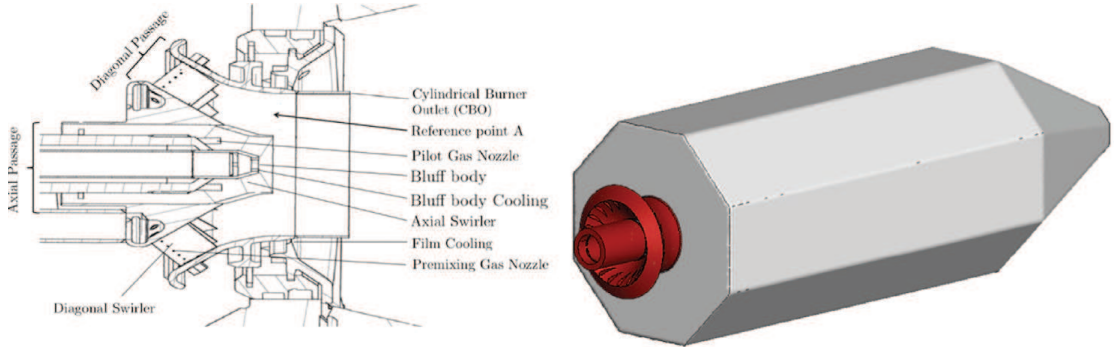

Fig. 24. Burner configuration (left) and combustion chamber (right) [164].

geometry and for fixed operating conditions, swirled flames can sometimes exhibit different shapes depending on the flame history. Hysteresis is commonly observed and one of the phenomena that can control the transition between the various states is CI: swirling flames are especially sensitive to hysteresis [160] because the recirculation zones (either the central recirculation zone (CRZ) or the outer recirculation zones (ORZ)) on which the flame stabilizes can contain cold or burnt gases, leading to (at least) two different stable states. Huang and Yang [161,162] performed an LES of the dump-stabilized flame of Seo [163] where ORZ contain fresh or burnt gases depending on the inlet air temperature. They showed that the transition from a flame where the ORZ is cold (left image in Fig. 23) to a flame where the ORZ is hot (right image in Fig. 23) was due to the increased flame speed induced by the higher inlet temperature.

No hysteresis is observed here (the transition takes place because the inlet temperature is changed) but similar state changes can also occur for the same regime, leading to hysteresis if CIs occur: Hermeth et al. [164] used LES to demonstrate that a turbine burner (typical of large power gas turbine systems, Fig. 24) installed in an octogonal laboratory chamber at Ansaldo Energia S.p.A can exhibit two stable states for one fixed regime and that CI can trigger a transition from one to the other.

Depending on the flame initialization strategies, the LES of Hermeth et al. [164] leads to two states. The topology of both states (*Detached* and *Attached*) can be visualized by plotting an isosurface of temperature ($T/T_{mean} = 1.3$, Fig. 25). The isosurface is colored by the normalized axial velocity. Velocities are non-dimensionalized by the bulk velocity. In the *Attached* state (Fig. 25 left), the CRZ is ignited, it contains burnt gases and the flame is stabilized on the central hub of the burner. In the *Detached* state (Fig. 25 right), the CRZ is not ignited and the flame is stabilized only by the ORZ, leading to a longer flame, weakly stabilized. Of course, temperature profiles for both states are totally different as shown in Fig. 26 right. Obviously, NOx emissions would also be vastly different.

In practice, experimentalists know that these two states exist, even though it is quite difficult to perform measurements in these large chambers. This transition can be triggered by any small change in operating conditions, by turbulent fluctuations or as tested by Hermeth et al. [164], by acoustic waves. This acoustic forcing may be due to a self-excited CI mode or to external forcing: Hermeth et al. [164] forced the air inlet of the combustor at various frequencies and amplitudes to investigate the response of the combustor state to acoustic waves.

In the absence of forcing, both states can be maintained for very long times. When acoustic

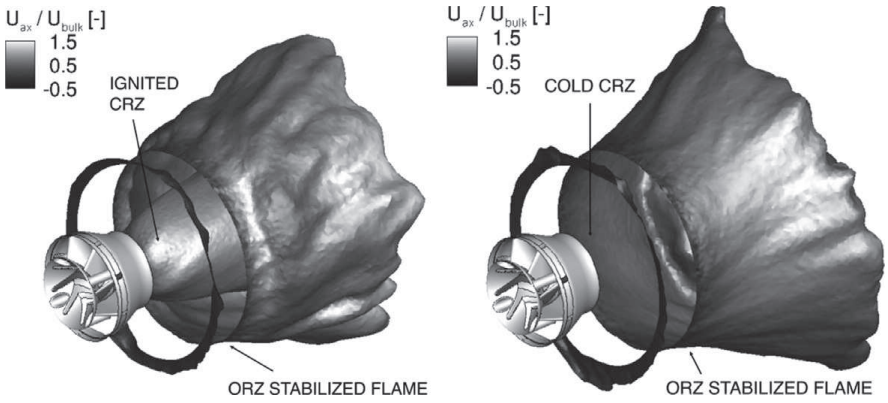

Fig. 25. Temperature iso-surface ($T/T_{mean} = 1.3$) colored by normalized axial velocity for the *Attached* state (left) and the *Detached* state (right) [164].

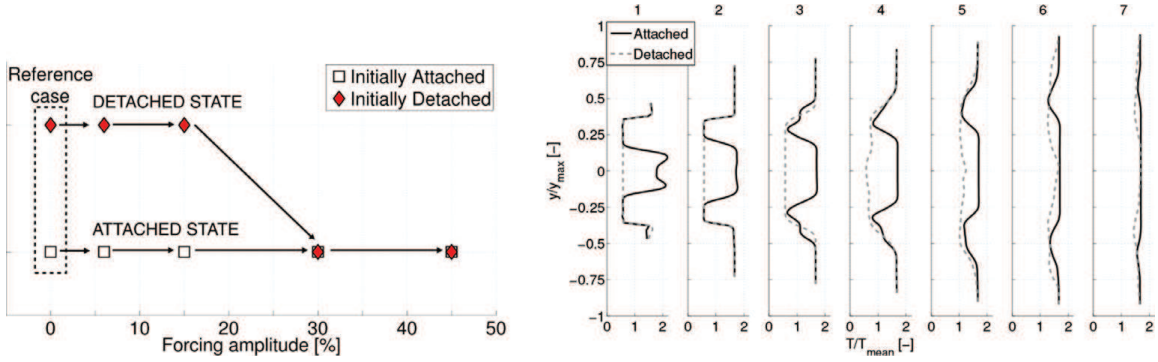

Fig. 26. Left: bifurcation diagram for the *Initially Attached* and *Initially Detached* flames as a function of the forcing amplitude. Right: mean temperature profiles for the *Attached* and *Detached* states.

forcing is applied, the *Attached* state is the most stable: even high levels of forcing cannot lead to a quenching of the ORZ and a transition to the *Detached* state as shown by the bifurcation diagram in Fig. 26 left. The *Detached* state, however, is sensitive to acoustic waves and if the burner is forced acoustically (at a frequency of the order of a few hundred Hz), the flame starts oscillating, invading the CRZ and finally stabilizing in the *Attached* state as shown by Fig. 27. This is obtained only for sufficiently high pulsation amplitudes (at least 15% of the mean velocity) (Fig. 26 left). At low forcing amplitudes, the *Detached* state only oscillates around its mean position.

4.6. UQ (Uncertainty Quantification) for combustion instabilities

An additional difficulty to predict CIs is the effect of uncertain parameters: most CI codes provide a bi-modal answer (yes or no) to the question 'is this burner stable or not?' A major question is then to know how robust this answer is to uncertainties, in other words to determine the probability that a mode will be stable or not, taking into account the uncertainties on input parameters. CIs are sensitive to many parameters that have unknown values or are even not identified: fuel composition, geometrical changes (due to manufacturing tolerances but also to wear-out phenomena during operation), air temperature, fuel spray characteristics, wall temperatures. The swirling flows used in most gas turbines are very sensitive [142,165,166]: a minute change of geometry in a swirler is sufficient for combustion to bifurcate from a stable quiet regime to an unstable one destroying the combustor in a few minutes. For solid rocket engines, out of ten (supposedly) identical engines, eight can be stable during tests and two unstable: identifying the source of this variation is a critical and challenging question. In the context of the introduction of alternative fuels (bio fuels for example or mixtures of gases) in combustors, UQ becomes mandatory: is it possible that by changing slightly the fuel composition or by mixing two fuels, a stable combustor might become unstable?

The UQ problem also extends to the simulation tools themselves and puts a new constraint on them: it is not enough to predict the stability map of a given combustor (the domain where this combustor can be operated safely) any more, it is also necessary to determine the precision associated to this prediction. Uncertainty sources are linked not only to physical parameters (geometry, regimes, impedances) but also to modeling issues (mesh size, numerical scheme accuracy, multiplicity of sub-models).

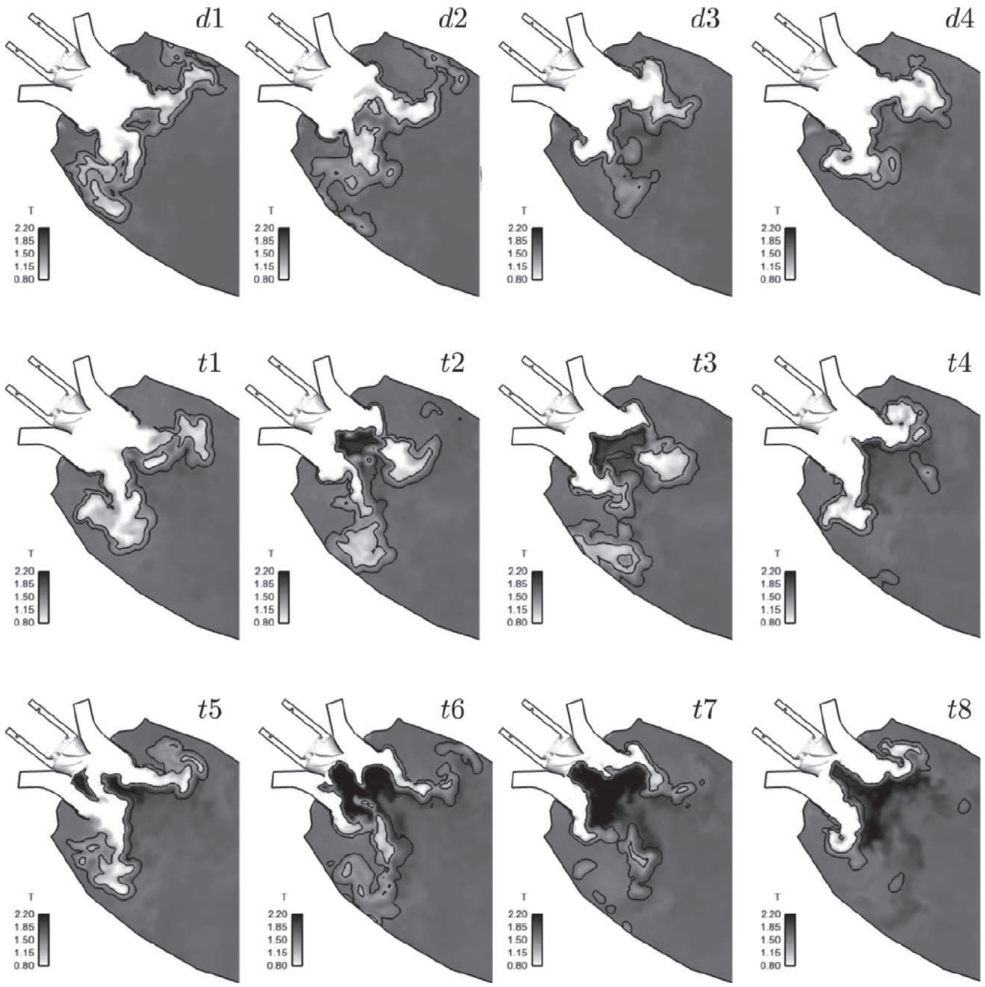

Fig. 27. Time sequence of normalized temperature field on the middle cut plane during the attachment sequence of the *Detached* flame at a pulsation amplitude of 45% [164].

The first difficulty to apply UQ tools to thermoacoustics is the large number of uncertain parameters that must be included: numerical parameters (mesh, physical submodels, boundary conditions) as well as physical parameters (geometry, chemistry, impedances). The well-known 'curse of dimensionality' (i.e. the fact that too many parameters are uncertain) hits the field of thermoacoustics directly because most simulation tools (Fig. 4) are expensive and cannot be run when too many input parameters have to be changed. For LES, this will probably be impossible for a long time. For TA codes, this is easier to imagine and certain tests show the benefits of this exercise: a proper approach to demonstrate the expected results of UQ for CI is to replace 3D solvers by a surrogate model.

For azimuthal modes discussed in Section 3, a good surrogate model for TA codes is the theoretical approach presented in Section 3.2. Since this model provides a fully analytical expression of the mode frequencies (Eq. (12)), it can be run for multiple input parameters at low cost. This was done recently for an annular chamber, with a single plenum and 19 burners [167]. The parameters that were supposed to be uncertain are the 38 parameters n_i and τ_i of the 19 burners. All other parameters were supposed to be fixed. Even for this reduced set of uncertain input parameters, a 38 dimension space is still a very large one and an active subspace method [168] was used to reduce this dimension before using UQ analysis. A typical result is displayed in Fig. 28: all burners are supposed to be submitted to independent fluctuations of 5% on n_i and 10% on τ_i which are typical of experimental uncertainties on FTFs (Dr D. Durox, private communication). A Monte Carlo method using 10000 samples was used to build the pdf of the mode growth rate and, from this value, measure the probability that the mode would be stable or not. The deterministic value (white square in Fig. 28) predicts stability. The UQ analysis, on the other hand, shows a wide pdf with unstable samples. Changing n_i's and τ_i's by only 5% and 10% leads to a wide range of growth rates, from $-35\tilde{}s^{-1}$ to $+15\tilde{}s^{-1}$ and an overall probability of instability of 39%. It is a sobering observation indicating that small uncertainties on input data of the stability analysis (the 38 values used for n_i and on τ_i's) can lead to a result that is almost useless: the deterministic result predicts stability but this result has a 40% probability to be wrong.

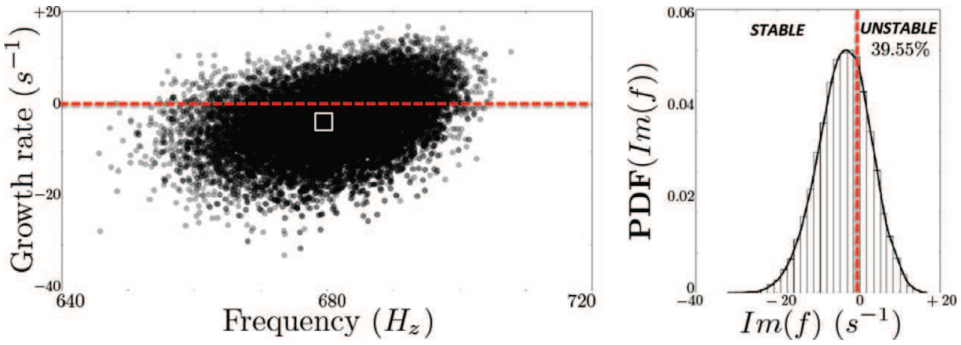

Fig. 28. UQ analysis of the growth rate of the first azimuthal mode vs real frequency in an annular chamber taking into account a 10% uncertainty on the 38 input parameters (n_i and τ_i for each burner).

5. Conclusions

Real engines offer an immense field of investigation for combustion instabilities because their complexity reveals mechanisms that cannot be captured in academic laboratory set-ups. This review has focused on a few questions that are specific to gas turbine engines such as the effects of heat losses, of flame bifurcations or of azimuthal modes that can be found only in annular chambers. Paradoxically, as the complexity of the configuration increases when real engines are considered, this review shows that the importance of theory increases: linear stability analysis of swirled flows, acoustic network descriptions of azimuthal modes, uncertainty quantifications and symmetry breaking are mandatory notions to tackle instabilities in real engines. Of course, LES has changed the field by allowing high-fidelity computations of real engines but LES alone cannot solve the overarching problem in this domain: understand CI to control them. This can be achieved only by combining LES results with careful experiments, theory and field data.

Acknowledgments

The research leading to these results has received funding from the European Research Council under the European Union's Seventh Framework Programme (FP/2007-2013)/ERC grant agreement ERC-AdG 319067-INTECOCIS. The support of the Center for Turbulence Research and of INCITE and PRACE programs, which provided CPU resources, is also gratefully acknowledged.

References

[1] J.C. Oefelein, V. Yang, *J. Prop. Power* 9 (5) (1993) 657–677.
[2] S. Ducruix, T. Schuller, D. Durox, S. Candel, *J. Prop. Power* 19 (5) (2003) 722–734.
[3] S. Ducruix, T. Schuller, D. Durox, S. Candel, *Prog. Energy Comb. Sci.* 210 (2005) 179.
[4] T. Lieuwen, *J. Fluid Mech.* 435 (2001) 289–303.
[5] F. Boudy, D. Durox, T. Schuller, S. Candel, *Proc. Combust. Inst.* 33 (2011) 1121–1128.
[6] C.O. Paschereit, W. Polifke, B. Schuermans, O. Mattson, *J. Eng. Gas Turbine Power* 124 (2002) 239–247.
[7] V. Kornilov, R. Rook, J. ten Thije Boonkkamp, L. de Goey, *Combust. Flame* 156 (2009) 1957–1970.
[8] K. Kedia, A. Ghoniem, *Proc. Combust. Inst.* 34 (1) (2013) 921–928.
[9] A. Cuquel, D. Durox, T. Schuller, *C. R. Acad. Sci. Mecanique* 341 (2013) 171–180.
[10] Y. Huang, H.G. Sung, S.Y. Hsieh, V. Yang, *J. Prop. Power* 19 (5) (2003) 782–794.
[11] P. Weigand, W. Meier, X. Duan, W. Stricker, M. Aigner, *Combust. Flame* 144 (1–2) (2006) 205–224.
[12] S. Wang, V. Yang, G. Hsiao, S.-Y. Hsieh, H.C. Mongia, *J. Fluid Mech.* 583 (2007) 99–122.
[13] W. Meier, P. Weigand, X. Duan, R. Giezendanner-Thoben, *Combust. Flame* 150 (1–2) (2007) 2–26.
[14] L.Y.M. Gicquel, G. Staffelbach, T. Poinsot, *Prog. Energy Combust. Sci.* 38 (6) (2012) 782–817.
[15] M. Stohr, I. Boxx, C.D. Carter, W. Meier, *Combust. Flame* 159 (8) (2012) 2636–2649.
[16] S. Terhaar, K. Oberleithner, C.O. Paschereit, *Proc. Combust. Inst.* 35 (2014).
[17] P.L. Therkelsen, J.E. Portillo, D. Littlejohn, S.M. Martin, R.K. Cheng, *Combust. Flame* 160 (2) (2013) 307–321.
[18] M. Bauerheim, G. Staffelbach, N. Worth, J. Dawson, L. Gicquel, T. Poinsot, *Proc. Combust. Inst.* 35 (3) (2015) 3355–3363.
[19] F.E.C. Culick, P. Kuentzmann, *Unsteady Motions in Combustion Chambers for Propulsion Systems*, NATO Research and Technology Organization, 2006.
[20] J. O'Connor, V. Acharya, T. Lieuwen, *Prog. Energy Combust. Sci.* 49 (C) (2015) 1–39.
[21] Y. Mery, S. Ducruix, P. Scouflaire, S. Candel, *Comptes Rendus Mécanique* 337 (6) (2009) 426–437.
[22] Y. Méry, L. Hakim, P. Scouflaire, L. Vingert, S. Ducruix, S. Candel, *Comptes Rendus Mécanique* 341 (1) (2013) 100–109.
[23] L. Hakim, T. Schmitt, S. Ducruix, S. Candel, *Combust. Flame* 162 (10) (2015) 3482–3502.
[24] L. Crocco, *J. Am. Rocket Soc.* 21 (1951) 163–178.
[25] L. Crocco, S.I. Cheng, *Theory of Combustion Instability in Liquid Propellant Rocket Motors*, vol. Agardograph No 8, Butterworths Science, 1956.
[26] D.J. Harrje, F.H. Reardon, Liquid Propellant Rocket Instability, *Technical Report Report SP-194*, NASA, 1972.

[27] S. Hochgreb, D.J.C. Dennis, I. Ayranci, W. Bainbridge, S. Cant, in: Proceedings of ASME Turbo Expo 2013—GT2013-9531, 2013.
[28] M.d.l.C. García, E. Mastorakos, A.P. Dowling, *Combust. Flame* 156 (2) (2009) 374–384.
[29] J. Kopitz, A. Huber, T. Sattelmayer, W. Polifke, in: ASME GT2005-68797, Reno, NV, U.S.A., 2005.
[30] N. Worth, J. Dawson, *Proc. Combust. Inst.* 34 (2012) 1–8.
[31] J.F. Bourgouin, D. Durox, J.P. Moeck, T. Schuller, S. Candel, *Proc. Combust. Inst.* 35 (3) (2015) 3237–3244.
[32] W. Krebs, G. Walz, S. Hoffmann, in: 5th AIAA Aeroacoustics Conference AIAA 99-1971, 1999.
[33] P. Berenbrink, S. Hoffmann, in: ASME Turbo Expo 2001. Paper 2001-GT-42, 2001.
[34] W. Krebs, P. Flohr, B. Prade, S. Hoffmann, *Combust. Sci. Technol.* 174 (2002) 99–128.
[35] S. Candel, *Proc. Combust. Inst.* 29 (1) (2002) 1–28.
[36] T. Lieuwen, V. Yang, Combustion Instabilities in Gas Turbine Engines. Operational Experience, Fundamental Mechanisms and Modeling, Prog. in Astronautics and Aeronautics AIAA, vol. 210, 2005.
[37] L.P.H. De Goey, J.A. van Oijen, V.N. Kornilov, J.H.M. ten Thije Boonkkamp, *Proc. Combust. Inst.* 33 (1) (2011) 863–886.
[38] T. Poinsot, A. Trouvé, D. Veynante, S. Candel, E. Esposito, *J. Fluid Mech.* 177 (1987) 265–292.
[39] M. Ihme, H. Pitsch, H. Bodony, *Proc. Combust. Inst.* 32 (2009) 1545–1554.
[40] S. Candel, D. Durox, S. Ducruix, A. Birbaud, N. Noiray, T. Schuller, *Int. J. Acoust.* 8 (2009) 1–56.
[41] L. Rayleigh, *Nature* July 18 (1878) 319–321.
[42] A.A. Putnam, J.M. Beer, Combustion Driven Oscillations in Industry, Fuel and Energy Science Series, American Elsevier, 1971.
[43] F.A. Williams, *Combustion Theory*, Benjamin Cummings, Menlo Park, CA, 1985.
[44] E.W. Price, in: 12th Symp. (Int.) on Combustion, The Combustion Institute, Pittsburgh, 1969, pp. 101–113.
[45] M. Barrère, F.A. Williams, *Proc. Combust. Inst.* 12 (1968) 169–181.
[46] W. Strahle, *Prog. Energy Combust. Sci.* 4 (1978) 157–176.
[47] B.D. Mugridge, *J. Sound Vib.* 70 (1980) 437–452.
[48] V. Yang, F.E.C. Culick, *Combust. Sci. Technol.* 45 (1986) 1–25.
[49] D.G. Crighton, A.P. Dowling, J.E.F. Williams, M. Heckl, F. Leppington, Modern Methods in Analytical Acoustics, Lecture Notes, Springer Verlag, New-York, 1992.
[50] S. Candel, C. Huynh., T. Poinsot, in: NATO ASI Series, Kluwer Academic Publishers, Dordrecht, 1996, pp. 83–112.
[51] A.P. Dowling, *J. Sound Vib.* 180 (4) (1995) 557–581.
[52] C. Martin, L. Benoit, Y. Sommerer, F. Nicoud, T. Poinsot, *AIAA J.* 44 (4) (2006) 741–750.
[53] A.S. Morgans, S.R. Stow, *Combust. Flame* 150 (4) (2007) 380–399.
[54] P.L. Rijke, *Phil. Mag.* 17 (1859a) 419–422.
[55] P.L. Rijke, *Ann. Phys.* 107 (1859b) 339.
[56] J. Moeck, M. Oevermann, R. Klein, C. Paschereit, H. Schmidt, *Proc. Combust. Inst.* 32 (2009) 1199–1207.
[57] J. Moeck, M. Paul, C. Paschereit, in: ASME Turbo Expo 2010 GT2010-23577, 2010.
[58] E. Courtine, L. Selle, T. Poinsot, *Combust. Flame* 162 (2015) 4331–4341.
[59] T. Poinsot, D. Veynante, *Theoretical and Numerical Combustion*, third ed., 2011. www.cerfacs.fr/elearning
[60] M. Bauerheim, F. Nicoud, T. Poinsot, *Combust. Flame* 162 (1) (2015) 60–67.
[61] K. Truffin, T. Poinsot, *Combust. Flame* 142 (4) (2005) 388–400.
[62] T. Sayadi, P.J. Schmid, F. Richecoeur, D. Durox, *Phys. Fluids* 27 (3) (2015) 037102.
[63] N. Noiray, D. Durox, T. Schuller, S. Candel, *J. Fluid Mech.* 615 (2008) 139–167.
[64] D. Durox, T. Schuller, N. Noiray, S. Candel, *Proc. Combust. Inst.* 32 (1) (2009) 1391–1398.
[65] P. Palies, D. Durox, T. Schuller, S. Candel, *Combust. Flame* 158 (10) (2011) 1980–1991.
[66] T. Lieuwen, B.T. Zinn, *Proc. Combust. Inst.* 27 (1998) 1809–1816.
[67] T. Sattelmayer, *J. Eng. Gas Turbine Power* 125 (2003) 11–19.
[68] A. Birbaud, S. Ducruix, D. Durox, S. Candel, *Combust. Flame* 154 (3) (2008) 356–367.
[69] S. Camporeale, B. Fortunato, G. Campa, *J. Eng. Gas Turbine Power* 133 (1) (2011).
[70] F. Nicoud, L. Benoit, C. Sensiau, T. Poinsot, *AIAA J.* 45 (2007) 426–441.
[71] C. Pankiewitz, T. Sattelmayer, *J. Eng. Gas Turbine Power* 125 (3) (2003) 677–685.
[72] A.P. Dowling, S.R. Stow, *J. Prop. Power* 19 (5) (2003) 751–764.
[73] K. Kedia, H. Altay, A. Ghoniem, *Proc. Combust. Inst.* 33 (2011) 1113–1120.
[74] S. Ducruix, D. Durox, S. Candel, *Proc. Combust. Inst.* 28 (1) (2000) 765–773.
[75] P. Schmitt, T. Poinsot, B. Schuermans, K.P. Geigle, *J. Fluid Mech.* 570 (2007) 17–46.
[76] C. Fureby, *Flow Turbine Combust.* 84 (2010) 543–564.
[77] N. Noiray, M. Bothien, B. Schuermans, *Combust. Theory Model.* 15 (2011) 585–606.
[78] G. Bloxsidge, A. Dowling, N. Hooper, P. Langhorne, *AIAA J.* 26 (1988) 783–790.
[79] T. Poinsot, W. Lang, F. Bourienne, S. Candel, E. Esposito, *J. Prop. Power* 5 (1989) 14–20.
[80] G. Billoud, M. Galland, C. Huynh, S. Candel, *Combust. Sci. Technol.* 81 (1992) 257–283.
[81] J. Seume, N. Vortmeyer, W. Krause, J. Hermann, C. Hantschk, P. Zangle, S. Gleis, D. Vortmeyer, A. Orthmann, *J. Eng. Gas Turbines Power* 120 (1998) 721–726.
[82] N. Gourdain, L. Gicquel, M. Montagnac, O. Vermorel, M. Gazaix, G. Staffelbach, M. Garcia, J. Boussuge, T. Poinsot, *Comput. Sci. Discovery* 2 (2009a) 015003.
[83] N. Gourdain, L. Gicquel, G. Staffelbach, O. Vermorel, F. Duchaine, J.-F. Boussuge, T. Poinsot, *Comput. Sci. Discovery* 2 (1) (2009b) 28pp.
[84] G. Staffelbach, L. Gicquel, G. Boudier, T. Poinsot, *Proc. Combust. Inst.* 32 (2009) 2909–2916.
[85] P. Wolf, G. Staffelbach, L. Gicquel, J.-D. Muller, T. Poinsot, *Combust. Flame* 159 (11) (2012) 3398–3413.
[86] J. Bourgouin, D. Durox, J.P. Moeck, T. Schuller, S. Candel, in: ASME Turbo Expo 2013 GT2013-95010, 2013.
[87] N. Worth, J. Dawson, in: Proc. Combust. Inst., vol. 34, 2013, pp. 3127–3134.

[88] N. Noiray, B. Schuermans, *Proc. R. Soc. A: Math. Phys. Eng. Sci.* 469 (2151) (2012) 20120535.
[89] B. Schuermans, C. Paschereit, P. Monkewitz, in: 44th AIAA Aerospace Sciences Meeting and Exhibit, vol. AIAA paper 2006-0549, 2006.
[90] C. Sensiau, F. Nicoud, T. Poinsot, *Int. J. Aeroacoust.* 8 (1) (2009) 57–68.
[91] G. Ghirardo, M. Juniper, in: 2013-0232, 2013.
[92] N. Worth, J. Dawson, *Combust. Flame* 160 (11) (2013) 2476–2489.
[93] J.-F. Bourgouin, D. Durox, J.P. Moeck, T. Schuller, S. Candel, *J. Eng. Gas Turbine Power* 137 (2) (2015) 021503-11.
[94] F. Baillot, F. Lespinasse, *Combust. Flame* 161 (5) (2014) 1247–1267.
[95] J. O'Connor, T. Lieuwen, *J. Eng. Gas Turbine Power* 134 (011501-9) (2012) 134.
[96] J. Blimbaum, M. Zanchetta, T. Akin, V. Acharya, J. O'Connor, D. Noble, T. Lieuwen, *Int. J. Spray Combust. Dyn.* 4 (4) (2012) 275–298.
[97] V. Acharya, M. Malanoski, M. Aguilar, T. Lieuwen, *J. Eng. Gas Turbine Power* 136 (5) (2014) 051503-10.
[98] F. Lespinasse, F. Baillot, T. Boushaki, *C. R. Acad. Sci. Mec.* 341 (1–2) (2013) 110–120.
[99] J.-F. Parmentier, P. Salas, P. Wolf, G. Staffelbach, F. Nicoud, T. Poinsot, *Combust. Flame* 159 (7) (2012) 2374–2387.
[100] S. Evesque, W. Polifke, C. Pankiewitz, in: 9th AIAA/CEAS Aeroacoustics Conference, vol. AIAA Paper 2003–3182, 2003.
[101] M. Bauerheim, J.-F. Parmentier, P. Salas, F. Nicoud, T. Poinsot, *Combust. Flame* 161 (5) (2014) 1374–1389.
[102] L. Li, X. Sun, *Combust. Flame* 162 (3) (2015) 628–641.
[103] M. Bauerheim, P. Salas, F. Nicoud, T. Poinsot, *J. Fluid Mech.* 760 (2014) 431–465, doi:10.1017/jfm.2014.578.
[104] A. Davey, H. Salwen, *J. Fluid Mech.* 281 (1994) 357–369.
[105] J. Guckenheimer, A. Mahalov, *Phys. Rev. Lett.* 68 (1992) 2257.
[106] A. Sengissen, J.F.V. Kampen, R. Huls, G. Stoffels, J.B.W. Kok, T. Poinsot, *Combust. Flame* 150 (2007) 40–53.
[107] R. Garby, L. Selle, T. Poinsot, *C. R. Acad. Sci. Mec.* 341 (1–2) (2013) 220–229.
[108] K. Kedia, A. Ghoniem, *Combust. Flame* 162 (4) (2015) 1304–1315.
[109] R. Raun, M. Beckstead, *Combust. Flame* 94 (1993) 1–24.
[110] K.J. Bosschaart, L. de Goey, *Combust. Flame* 132 (1–2) (2003) 170–180.
[111] K.J. Bosschaart, L.P.H. De Goey, *Combust. Flame* 136 (3) (2004) 261–269.
[112] F. Duchaine, F. Boudy, D. Durox, T. Poinsot, *Combust. Flame* 158 (12) (2011) 2384–2394.
[113] D. Mejia, L. Selle, R. Bazile, T. Poinsot, *Proc. Combust. Inst.* 35 (3201–3208) (2014) 3.
[114] L. Boyer, J. Quinard, *Combust. Flame* 82 (1990) 51–65.
[115] M. Fleifil, A.M. Annaswamy, Z.A. Ghoneim, A.F. Ghoniem, *Combust. Flame* 106 (4) (1996) 487–510.
[116] S.H. Lee, J.G. Ih, K.S. Peat, *J. Sound Vib.* 303 (3–5) (2007) 741–752.
[117] R. Rook, L. de Goey, L. Somers, K. Schreel, R. Parchen, *Combust. Theory Model.* 6 (2) (2002) 223–242.
[118] M. Hoeijmakers, V. Kornilov, I.L. Arteaga, P. de Goey, H. Nijmeijer, *Combust. Flame* 161 (2014) 2860–2867.
[119] T. Emmert, S. Bomberg, W. Polifke, *Combust. Flame* 162 (1) (2015) 75–85.
[120] E. Courtine, L. Selle, F. Nicoud, W. Polifke, C.F. Silva, M. Bauerheim, T. Poinsot., in: Proc. of the Summer Program, Center of Turbulence Research, Stanford University/NASA, Ames, USA, 2014, pp. 169–178.
[121] F. Hussain, J. Jeong, *J. Fluid Mech.* 285 (1995) 69–94.
[122] A.L. Birbaud, D. Durox, S. Ducruix, S. Candel, *Phys. Fluids* 19 (2007) 013602.
[123] E. Motheau, L. Selle, F. Nicoud, *J. Sound Vib.* 333 (1) (2013) 246–262.
[124] E. Motheau, F. Nicoud, T. Poinsot, *J. Fluid Mech.* 749 (2014) 542–576.
[125] F.E. Marble, S. Candel, *J. Sound Vib.* 55 (1977) 225–243.
[126] M. Huet, A. Giauque, *J. Fluid Mech.* 733 (2013) 268–301.
[127] I. Duran, S. Moreau, *J. Fluid Mech.* 723 (2013) 190–231, doi:10.1017/jfm.2013.118.
[128] W. Lang, T. Poinsot, S. Candel, *Combust. Flame* 70 (1987) 281–289.
[129] K. McManus, T. Poinsot, S. Candel, *Prog. Energy Combust. Sci.* 19 (1993) 1–29.
[130] N. Tran, S. Ducruix, T. Schuller, *Proc. Combust. Inst.* 32 (2) (2009) 2917–2924.
[131] B. Cosic, B. Bobusch, J. Moeck, C. Paschereit, *J. Eng. Gas Turbine Power* 134 (2012) 061502-1.
[132] W.C. Strahle, *J. Fluid Mech.* 49 (1971) 399–414.
[133] A.P. Dowling, Y. Mahmoudi, *Proc. Combust. Inst.* 35 (1) (2015) 65–100.
[134] N.A. Cumpsty, F.E. Marble, *Proc. R. Soc. Lond. A* 357 (1977) 323–344.
[135] F. Bake, N. Kings, A. Fischer, R. I., *Int. J. Aeroacoust.* 8 (1–2) (2008) 125–142.
[136] F. Bake, C. Richter, B. Muhlbauer, N. Kings, I. Rohle, F. Thiele, B. Noll, *J. Sound Vib.* 326 (2009) 574–598.
[137] M. Leyko, F. Nicoud, T. Poinsot, *AIAA J.* 47 (11) (2009) 2709–2716.
[138] I. Duran, S. Moreau, T. Poinsot, *AIAA J.* 51 (1) (2013) 42–52.
[139] M.S. Howe, *J. Fluid Mech.* 659 (2010) 267–288.
[140] W. Ullrich, T. Sattelmayer, in: 21st AIAA CEAS Aeroacoustics Conference, 2015, pp. 1–19.
[141] F.E. Marble, S. Candel, *J. Sound Vib.* 55 (1977) 225–243.
[142] S. Candel, D. Durox, T. Schuller, J.-F. Bourgouin, J.P. Moeck, *Ann. Rev. Fluid Mech.* 46 (1) (2014) 147–173.
[143] I. Duran, M. Leyko, S. Moreau, F. Nicoud, T. Poinsot, *C. R. Acad. Sci. Mec.* 341 (1–2) (2013) 131–140.
[144] M. Leyko, I. Duran, S. Moreau, F. Nicoud, T. Poinsot, *J. Sound Vib.* 333 (23) (2014) 6090–6106.
[145] J. Eckstein, E. Freitag, C. Hirsch, T. Sattelmayer, *J. Eng. Gas Turbine Power* 128 (2) (2006) 264–270.
[146] W. Polifke, C. Paschereit, K. Döbbeling, *Int. J. Acoust. Vib.* 6 (3) (2001) 135–146.

[147] C.S. Goh, A.S. Morgans, *Combust. Sci. Technol.* 185 (2) (2013) 249–268.
[148] A.S. Morgans, C.S. Goh, J.A. Dahan, *J. Fluid Mech.* 733 (R2) (2013), doi:10.1017/jfm.2013.448.
[149] B. Emerson, J. O'Connor, M. Juniper, T. Lieuwen, *J. Fluid Mech.* 706 (2012) 219–250.
[150] M. Juniper, *J. Fluid Mech.* 565 (2006) 171–195.
[151] A. Steinberg, I. Boxx, M. Stöhr, C. Carter, W. Meier, *Combust. Flame* 157 (2010) 2250–2266.
[152] S. Terhaar, K. Oberleithner, C.O. Paschereit, *Combust. Sci. Technol.* 186 (7) (2014).
[153] K. Oberleithner, M. Stöhr, S.H. Im, C.M. Arndt, A.M. Steinberg, *Combust. Flame* 162 (8) (2015) 3100–3114.
[154] S. Roux, G. Lartigue, T. Poinsot, U. Meier, C. Bérat, *Combust. Flame* 141 (2005) 40–54.
[155] A. Ghani, T. Poinsot, L. Gicquel, J.-D. Muller, *Flow, Turbine Combust.* 96 (2016) 207–226, doi:10.1007/s10494-015-9654-9.
[156] K. Oberleithner, S. Schimek, C.O. Paschereit, *Combust. Flame* 162 (1) (2015) 86–99.
[157] J.O. Keller, L. Vaneveld, D. Korschelt, G.L. Hubbard, A.F. Ghoniem, J.W. Daily, A.K. Oppenheim, *AIAA J.* 20 (1981) 254–262.
[158] Y. Sommerer, D. Galley, T. Poinsot, S. Ducruix, F. Lacas, D. Veynante, *J. Turbine* 5 (2004) 037.
[159] I. Chterev, C.W. Foley, D. Foti, S. Kostka, A.W. Caswell, N. Jiang, A. Lynch, D.R. Noble, S. Menon, J.M. Seitzman, T.C. Lieuwen, *Combust. Sci. Technol.* 186 (8) (2014) 1041–1074.
[160] M.J. Tummers, A.W. Hübner, E.H.v. Veen, K. Hanjalić, T.H.v.d. Meer, *Combust. Flame* 156 (2) (2009) 447–459.
[161] Y. Huang, V. Yang, *Combust. Flame* 136 (2004) 383–389.
[162] Y. Huang, V. Yang, *Prog. Energy Combust Sci.* 35 (4) (2009) 293–364.
[163] S. Seo, *Parametric Study of Lean Premixed Combustion Instability in a Pressurized Model Gas Turbine Combustor*, Department of Mechanical Engineering, Pennsylvania State University, 1999 (Ph.D. thesis).
[164] S. Hermeth, G. Staffelbach, L.Y. Gicquel, V. Anisimov, C. Cirigliano, T. Poinsot, *Combust. Flame* 161 (1) (2014) 184–196.
[165] M. Vanierschot, E.V. den Bulck, *Exp. Thermal Fluid Sci.* 31 (6) (2007) 513–524.
[166] M. Falese, L.Y. Gicquel, T. Poinsot, *Comput. Fluids* 89 (2014) 167–178.
[167] M. Bauerheim, A. Ndiaye, P. Constantine, G. Iaccarino, S. Moreau, F. Nicoud, in: Proceedings of the CTR Summer Program, 2014, pp. 209–210.
[168] T. Chantrasmi, G. Iaccarino, *Int. J. Uncertainty Quantif.* 2 (2) (2012) 125–143.